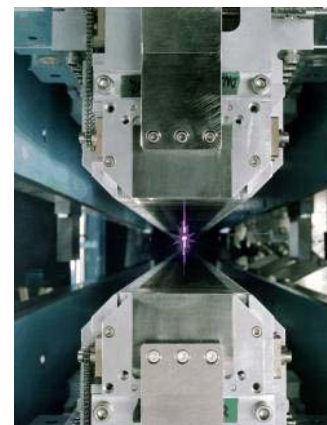




Alexei Fedorov

**Mass enhancement in the superconducting
state of $\text{Bi}_2\text{Sr}_2\text{CaCu}_2\text{O}_{8+d}$: new insights from
the photoemission**

Advanced Light Source, LBNL



ERNEST ORLANDO LAWRENCE
BERKELEY NATIONAL LABORATORY

Acknowledgements

BNL

P. Johnson

T. Valla

UConn

B. Wells

U. Colorado

D. Dessau

A. Gromko

Y-D. Chuang

UC Berkeley

A. Lanzara

G-H. Gweon

Outline

Photoemission:

- method
- instrumentation

Detecting coupling of
electrons to the collective modes
/e.g. phonons/ with photoemission:

- NbSe₂ /superconductor/
- TaSe₂ /CDW material/
- Gd(0001) /magnons/

New data on Bi₂Sr₂CaCu₂O_{8+d}
/high critical temperature superconductor/

Photoemission /inverse photoemission/

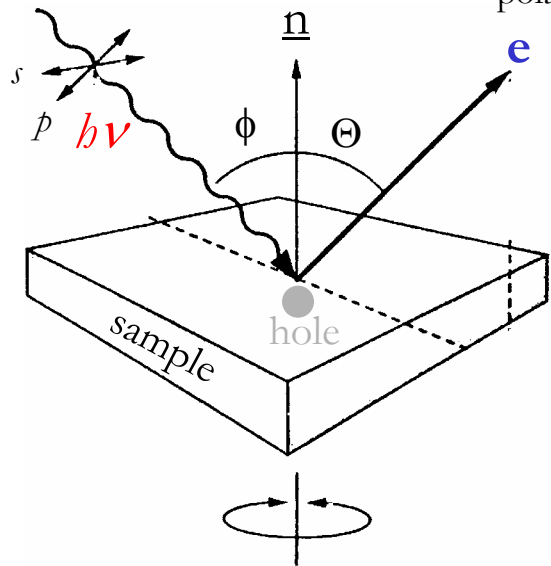
Experiment

Excitation Radiation

- photon energy
- polarization
- angle of incidence

Photoelectrons

- kinetic energy
- emission angle
- polarization



Important parameters:

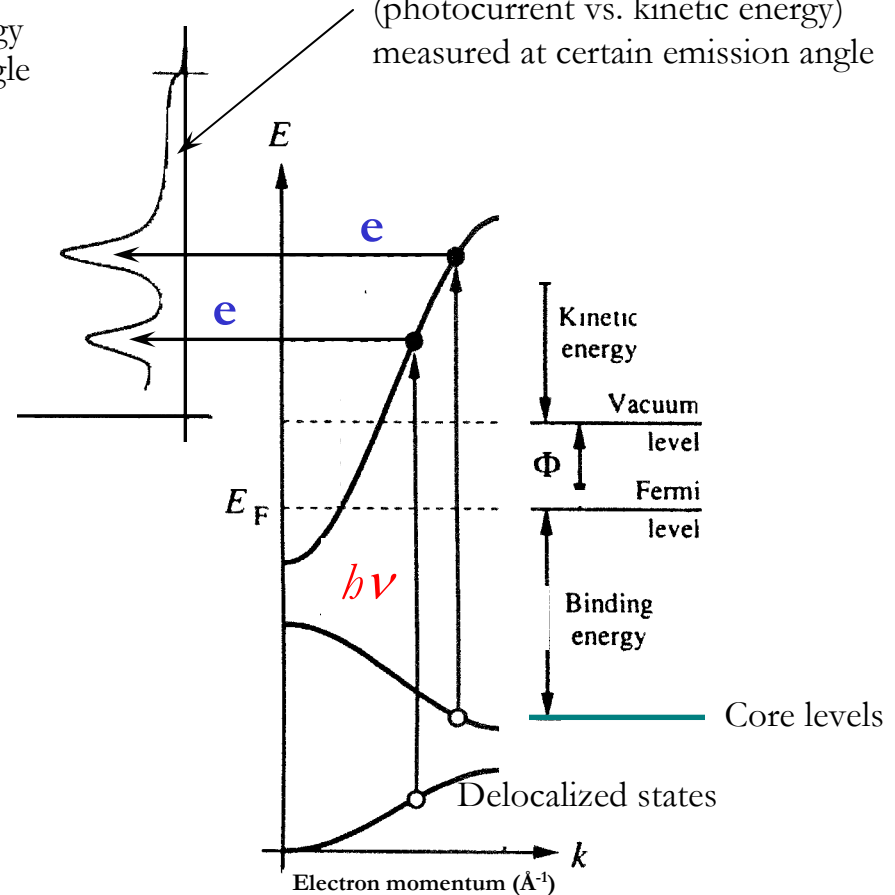
Energy resolution (~ 20 meV)

Angular resolution ($\sim 2^\circ$)

Data

Energy Distribution Curves

(photocurrent vs. kinetic energy)
measured at certain emission angle



Aim: learn Electronic structure or Chemical composition

Approach: fitting Data using appropriate models

Surface core level shifts in 4-f metals

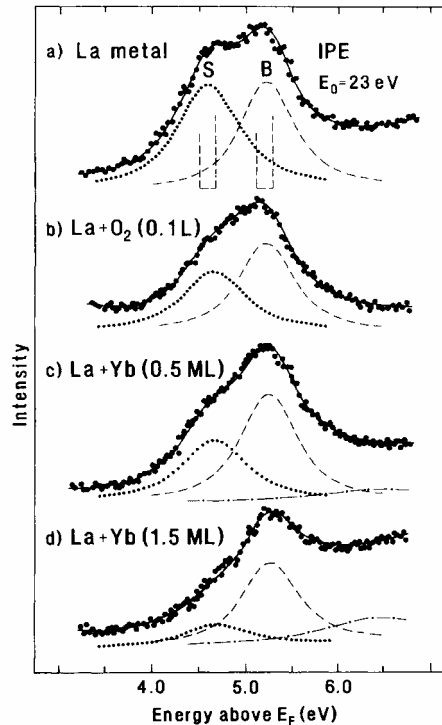


FIG. 2. Inverse photoemission spectra in the region of the $4f^1$ electron-addition state, taken at a primary electron energy of $E_0 = 23$ eV: (a) a clean surface of La metal; (b) after exposure to 0.1 L of oxygen; after coverage by (c) 0.5 monolayer (ML) of Yb and (d) 1.5 ML of Yb. The solid curves through the data points are the results of least-squares fits; for details see text.

A.V. Fedorov et al., PRL 70, 1719 (1992)

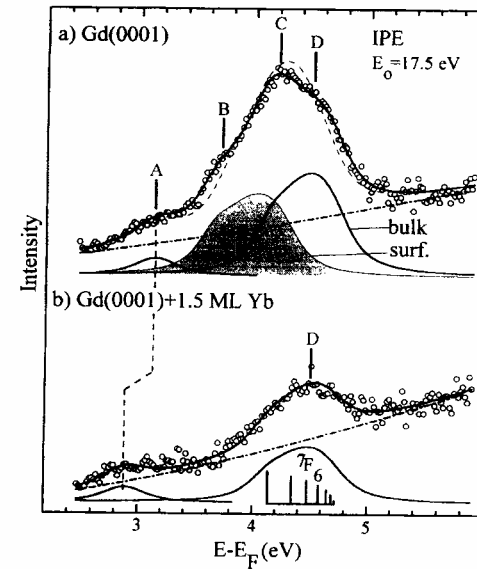
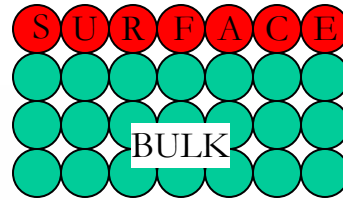


FIG. 1. IPE spectra of Gd(0001) in the region of the $4f^8$ electron-addition state, taken at a primary electron energy of $E_0 = 17.5$ eV: (a) clean Gd(0001) surface; (b) after coverage by 1.5 ML of Yb metal. Spectral features B, C, and D of clean Gd(0001) originate from $4f^8$ electron-addition states in the topmost surface layer (shaded) and in the bulk (solid curve); the vertical-bar diagram in (b) gives the energies and relative intensities of the individual 7F_J bulk multiplet components. The solid curves through the data points in (a) and (b) represent the results of the best least-squares fits. The dashed curve in (a) was obtained in a fit where $\delta_s^{sa} = \delta_s^{sr}$ was assumed. For details see text.

A.V. Fedorov et al., PRL 73, 601 (1994)

Electronic structure of high temperature superconductor and ferromagnetic Gd

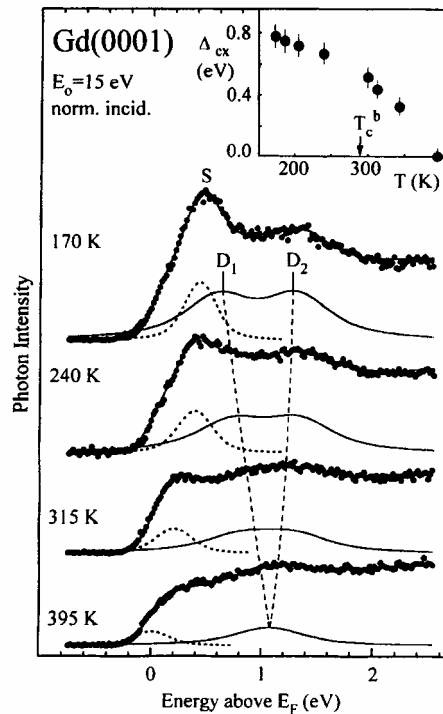


FIG. 4. Least-squares-fit analysis of selected inverse-photoemission spectra of Gd(0001) from Fig. 1 (for details, see text). The inset gives the exchange splitting Δ_{ex} as a function of temperature.

A.V. Fedorov et al., PRB 50, 2739 (1994)

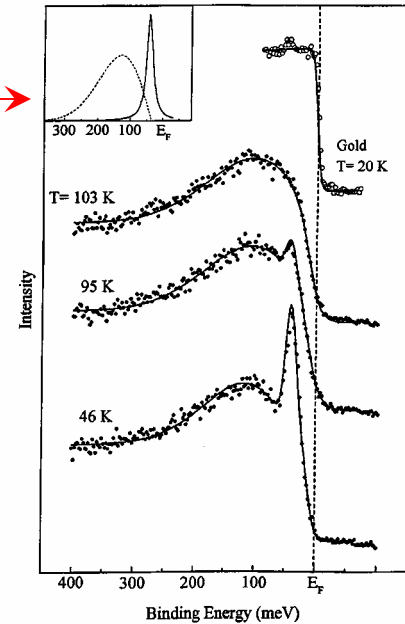


FIG. 2. Sample spectra at different temperatures showing the fit obtained using the two functions and background described in the text. The inset shows the two functions used in the fitting procedure. The parameter Δ_0 used in the latter fitting represents the separation of the leading edge of the broad peak from E_F , the Fermi level. The upper spectrum represents the Fermi edge obtained from an evaporated gold film.

VOLUME 82, NUMBER 10

PHYSICAL REVIEW LETTERS

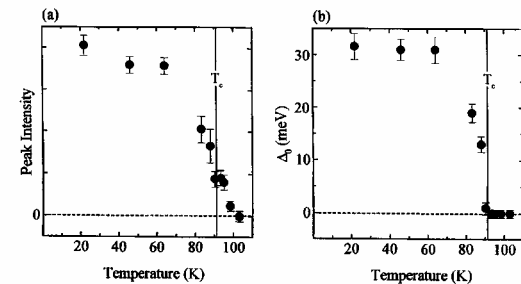
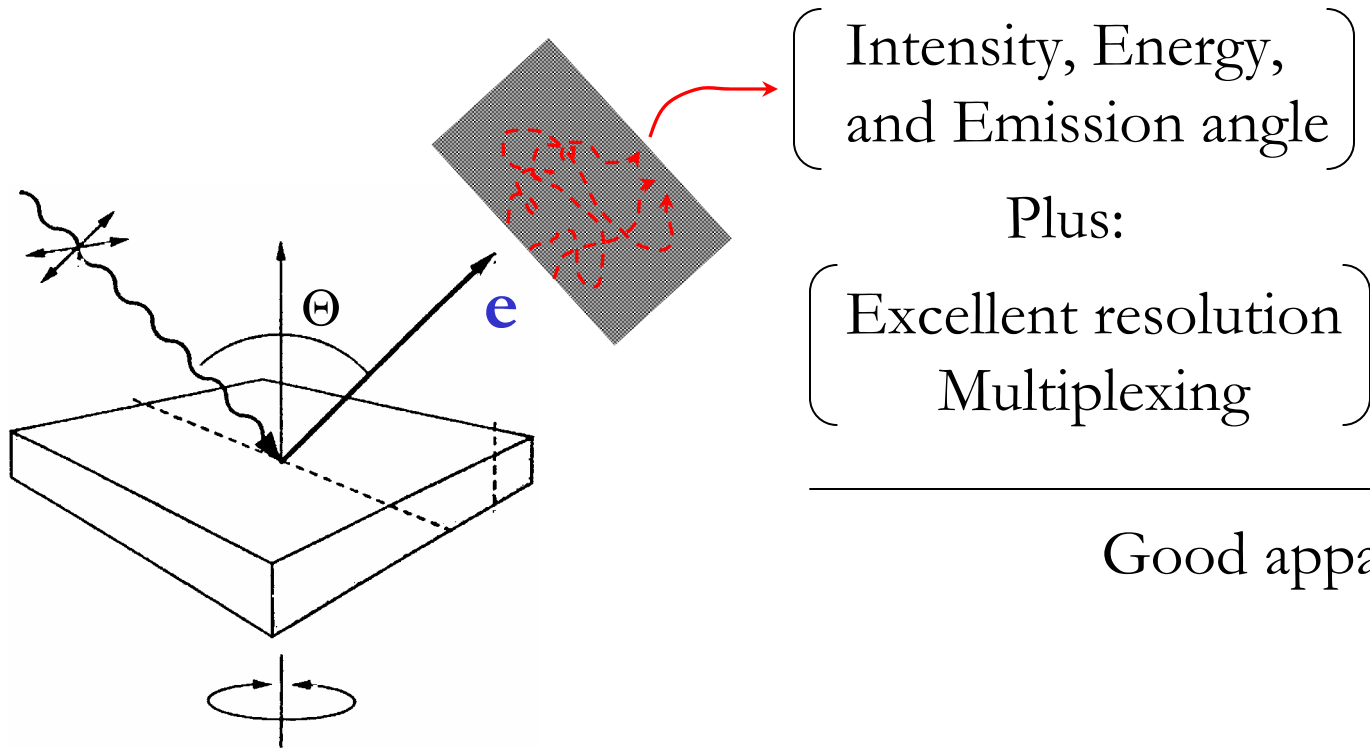


FIG. 3. (a) Intensity of the sharp peak as a function of the sample temperature. The transition temperature T_c is indicated. (b) The gap, Δ_0 , between the leading edge of the broad peak and the Fermi level as obtained from the fitting procedure.

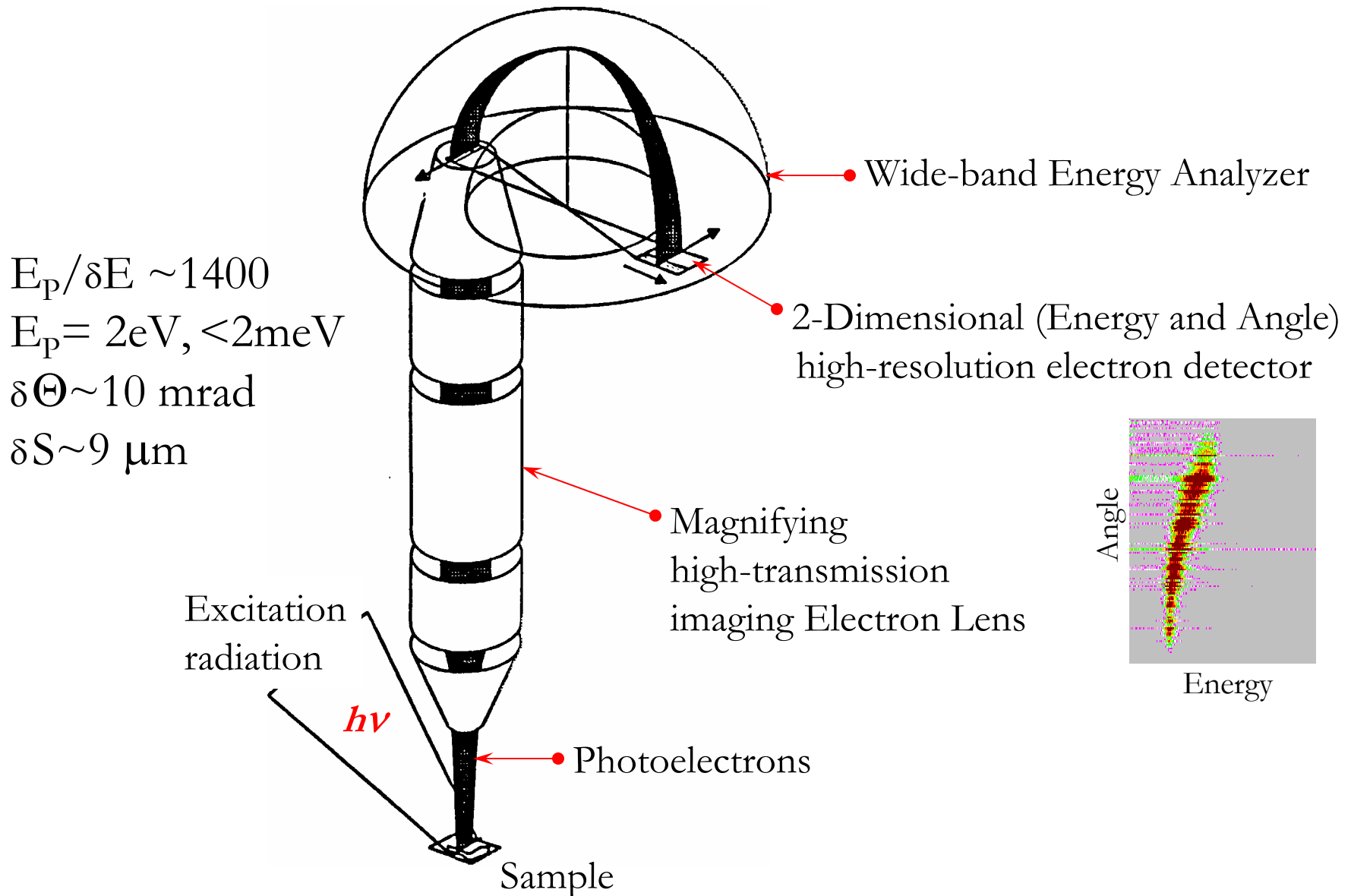
A.V. Fedorov et al., PRL 82, 2179 (1999)

What is an electron spectrometer?



Good apparatus

New Instrumentation from Gammadata-Scienta



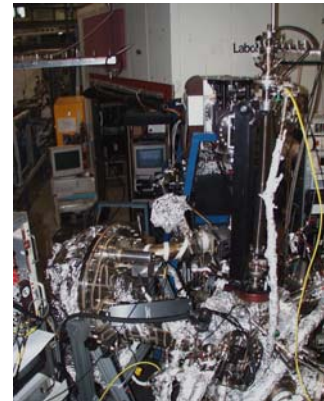
Other synchrotrons also have it:

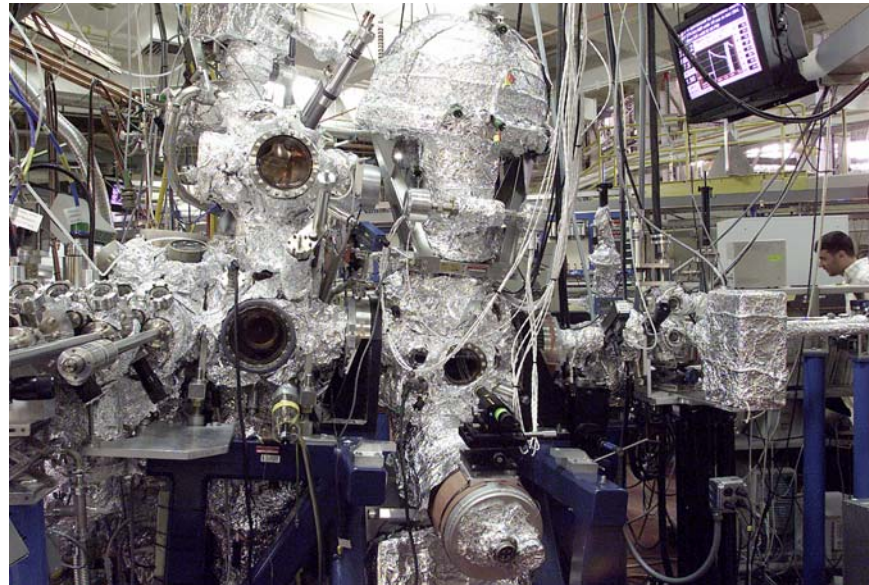
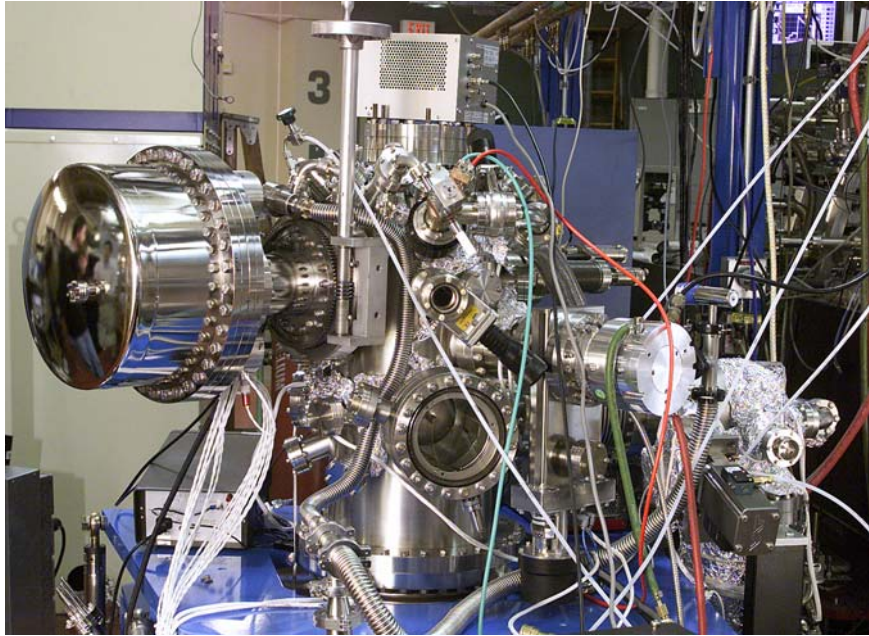
NSLS, Brookhaven: SES-200, SES-2002

SSRL, Stanford: SES-200, SES-2002

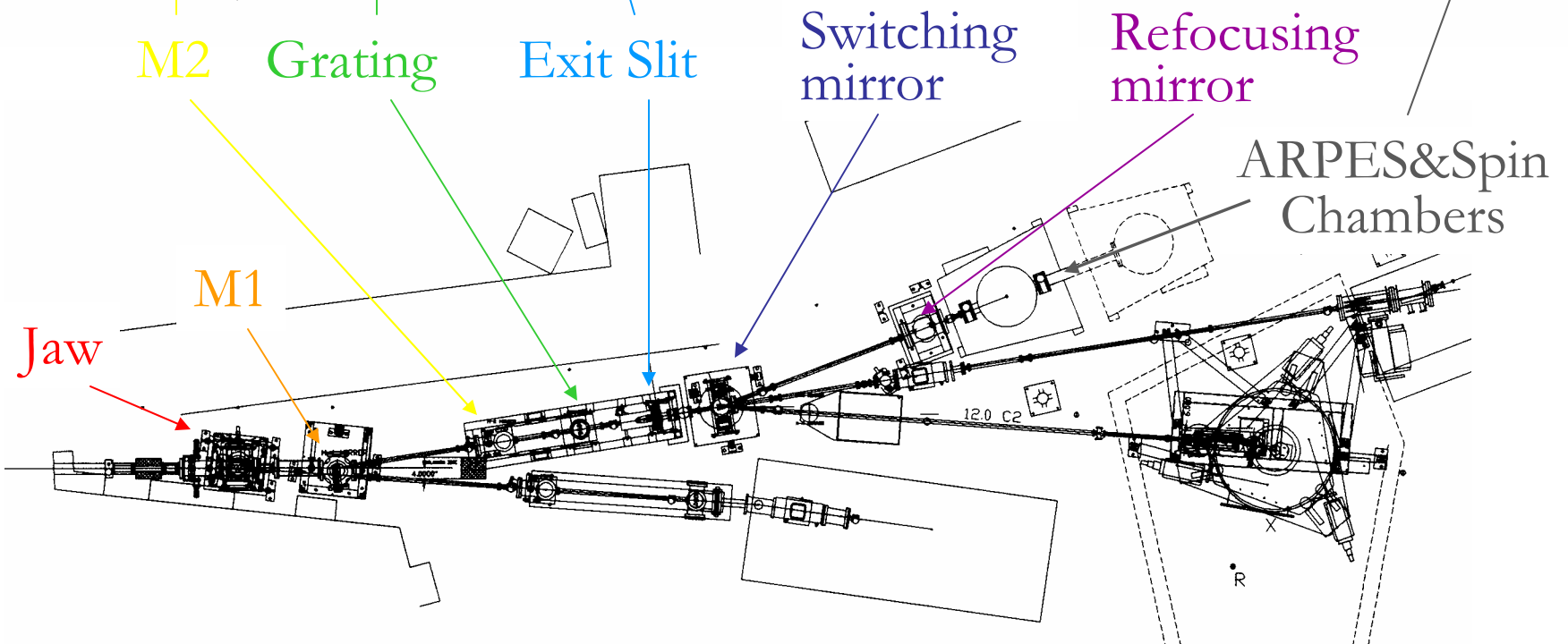
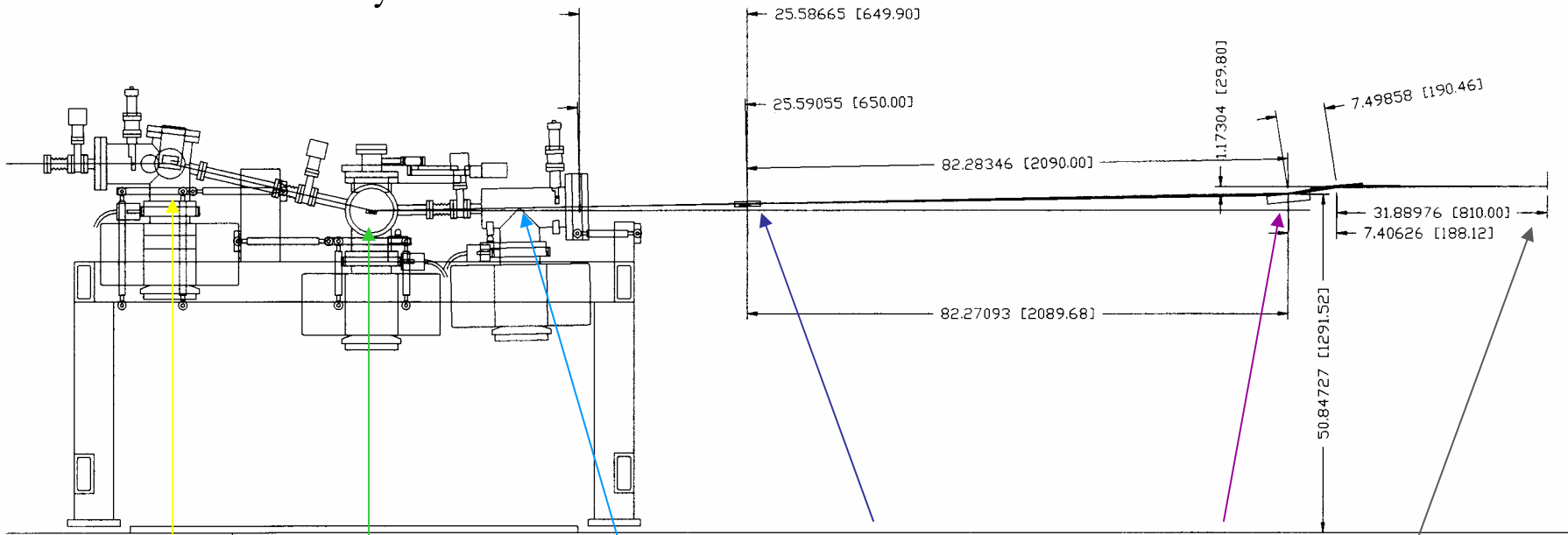
SRC, Stoughton: SES-200, SES-50, SES-2002

CAMD, Baton Rouge: SES-200





BL 12.0.1-1 Layout



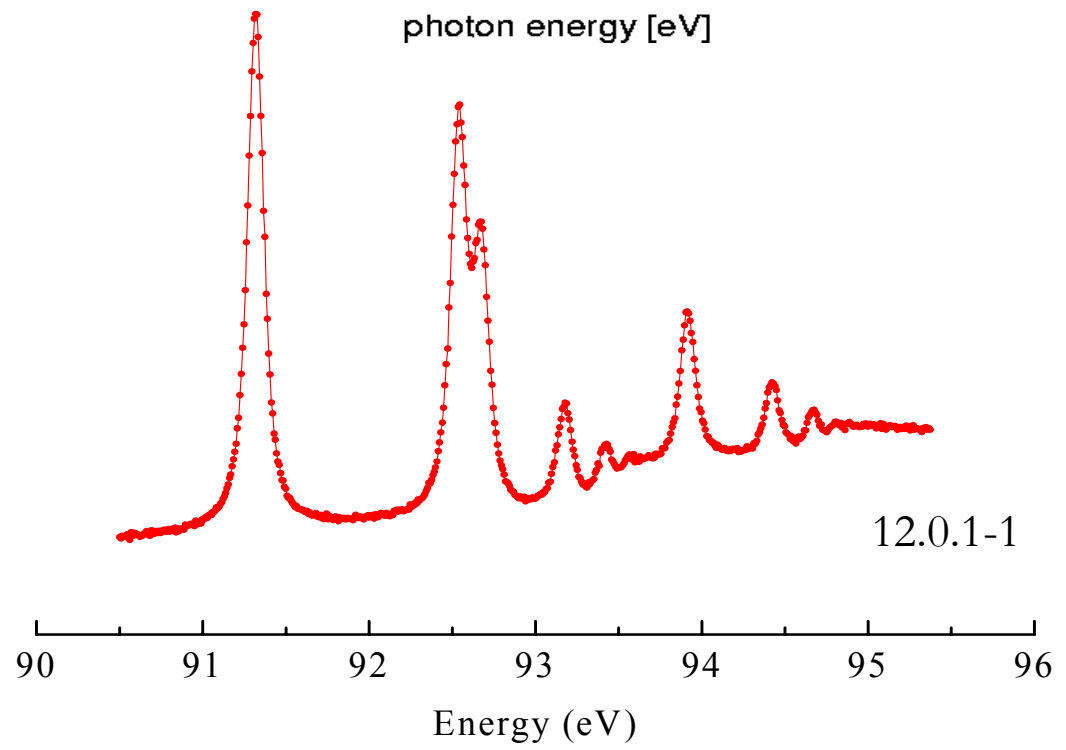
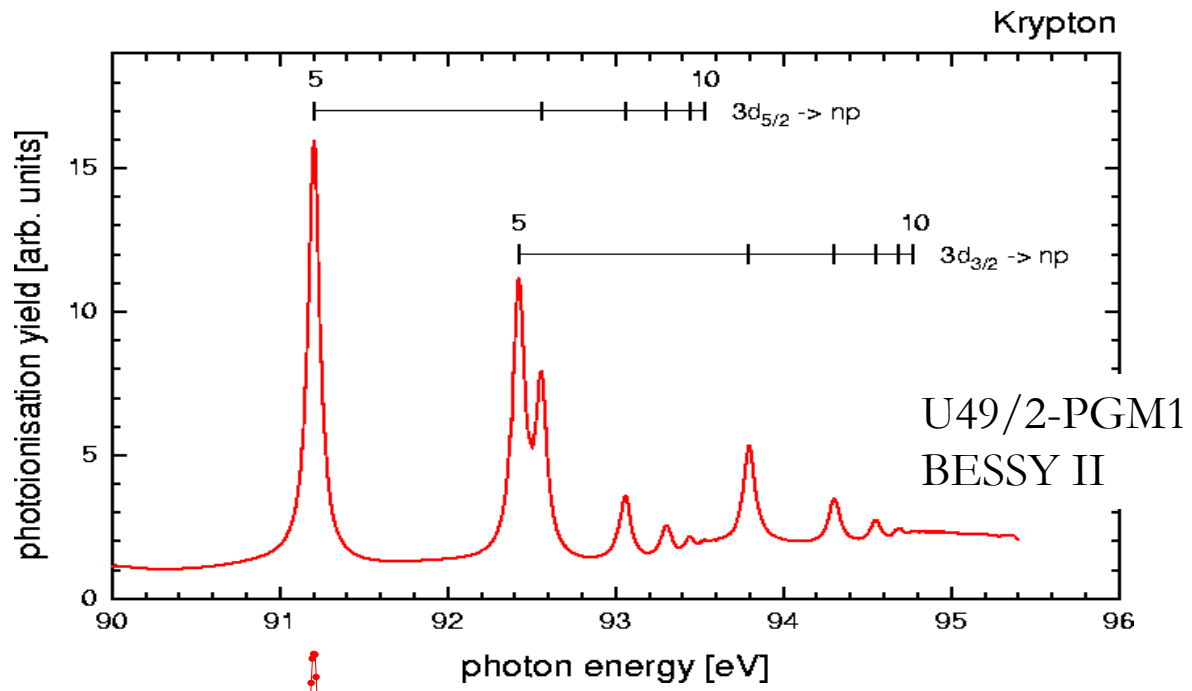
What is 12.0.1-1 for?

1. Angle-resolved photoemission /SES100/
2. Spin-resolved photoemission /SES200/
3. Anything else which needs photons

Who is in?



1. Univ. of Colorado /D. Dessau/
2. Advanced Light Source /Z. Hussain, A. Fedorov/
3. Stanford University / Z.X. Shen/
4. Anybody else who needs photons



Polarizer is on sale at Physical Science Laboratories, U. of Wisconsin-Madison

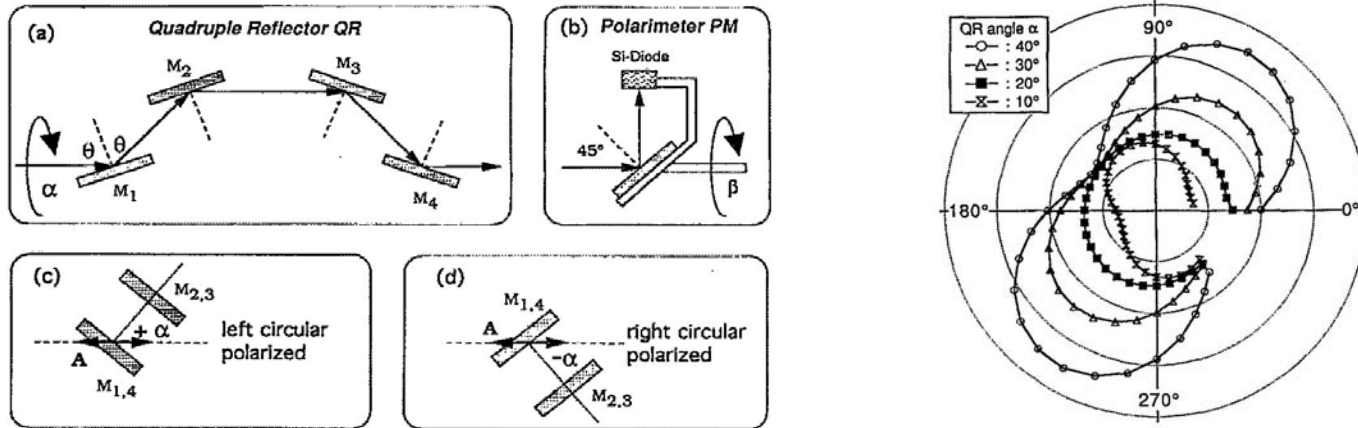


FIG. 1. (a) Schematic of the QR layout. (b) Schematic of the 45° -PM layout. (c) and (d) QR orientation for LCP and RCP.

FIG. 4. Intensity measurements with the 45° PM for different angles of rotation α of the QR. The angle of incidence was $\theta=78^\circ$ and the photon energy was $h\nu=25$ eV.

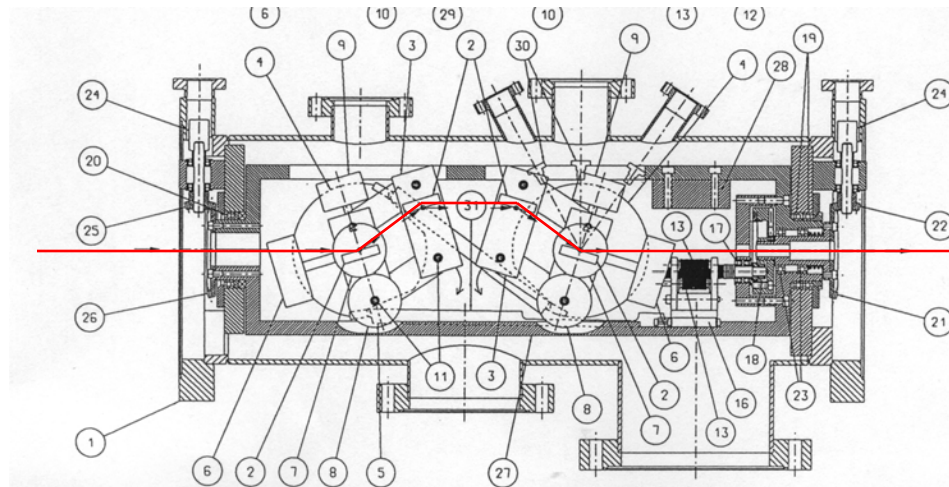
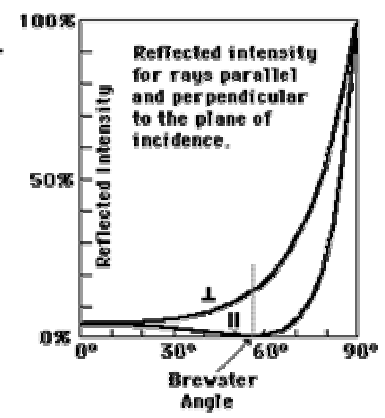
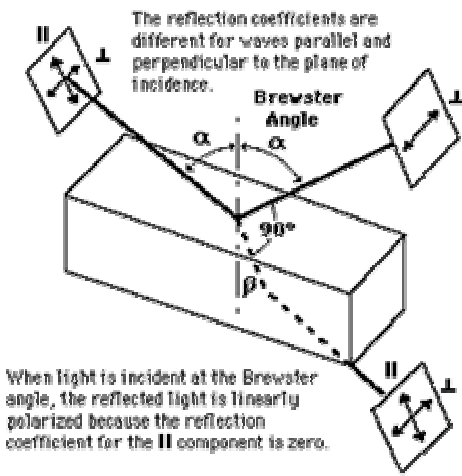
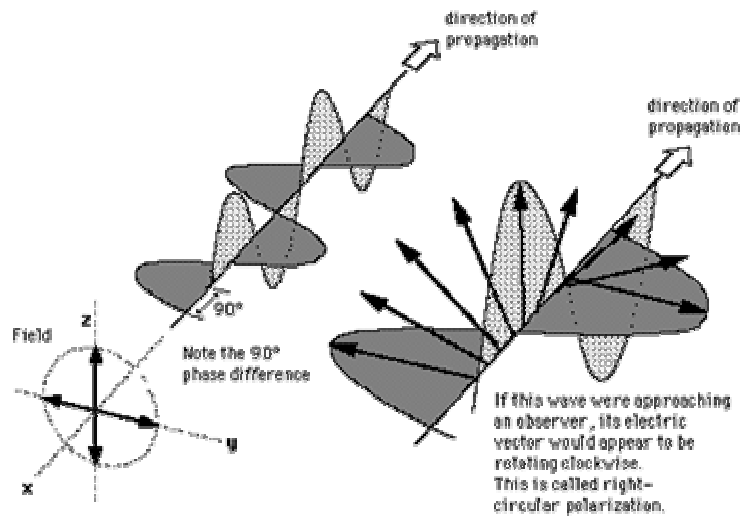


Fig. 7. (a) Top view of the mechanical layout of the quadruple reflector housing mechanism. (b) Side view of the polarizer



Why?

RAPID COMMUNICATIONS

PHYSICAL REVIEW B

VOLUME 61, NUMBER 6

1 FEBRUARY 2000-II

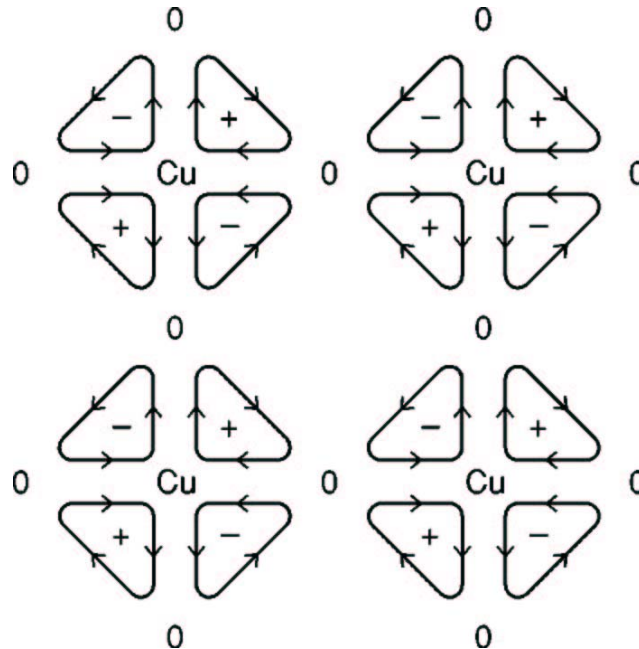
Proposal for an experiment to test a theory of high-temperature superconductors

C. M. Varma

Bell Laboratories, Lucent Technologies, Murray Hill, New Jersey 07974

(Received 21 October 1999)

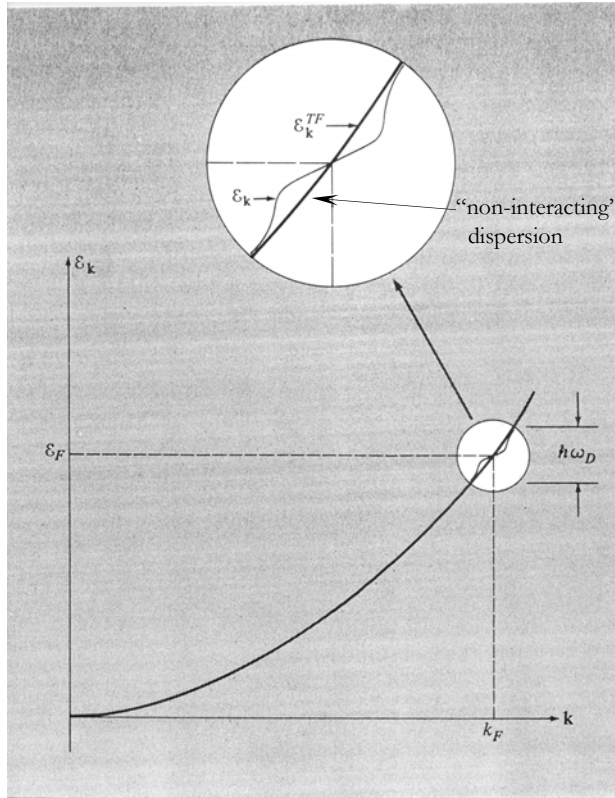
A theory for the phenomena observed in copper-oxide based high-temperature superconducting materials derives an elusive time-reversal and rotational symmetry-breaking order parameter for the observed pseudogap phase ending at a quantum-critical point near the composition for the highest T_c . An experiment is proposed to observe such a symmetry breaking. It is shown that angle-resolved photoemission yields a current density which is different for left and right circularly polarized photons. The magnitude of the effect and its momentum dependence is estimated. Barring the presence of domains of the predicted phase, an asymmetry of about 0.1 is predicted at low temperatures in moderately underdoped samples.



Electron-phonon coupling

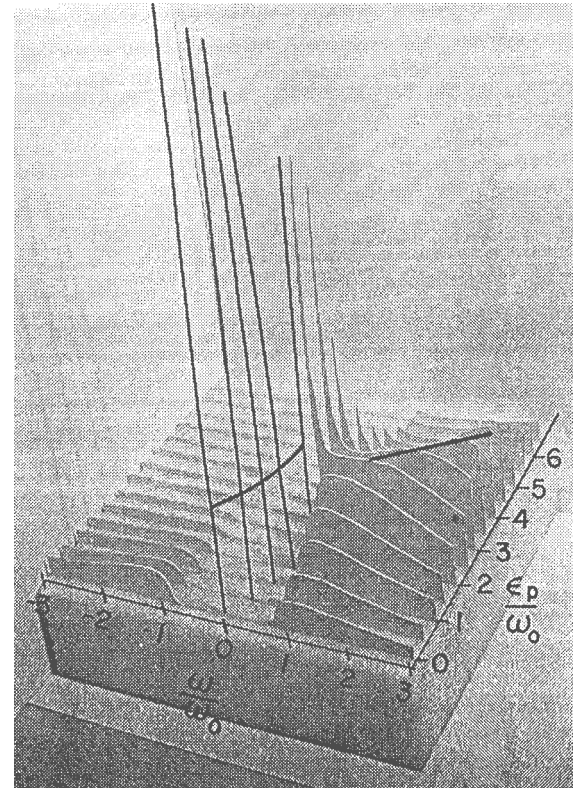
$$\text{Spectral function: } A(k, \omega) \sim \frac{|\operatorname{Im} \Sigma(k, \omega)|}{[\hbar\omega - e_k - \operatorname{Re} \Sigma(k, \omega)]^2 + \operatorname{Im} \Sigma(k, \omega)^2}$$

Dispersion relations



Solid State Physics
Neil W. Ashcroft
N. David Mermin

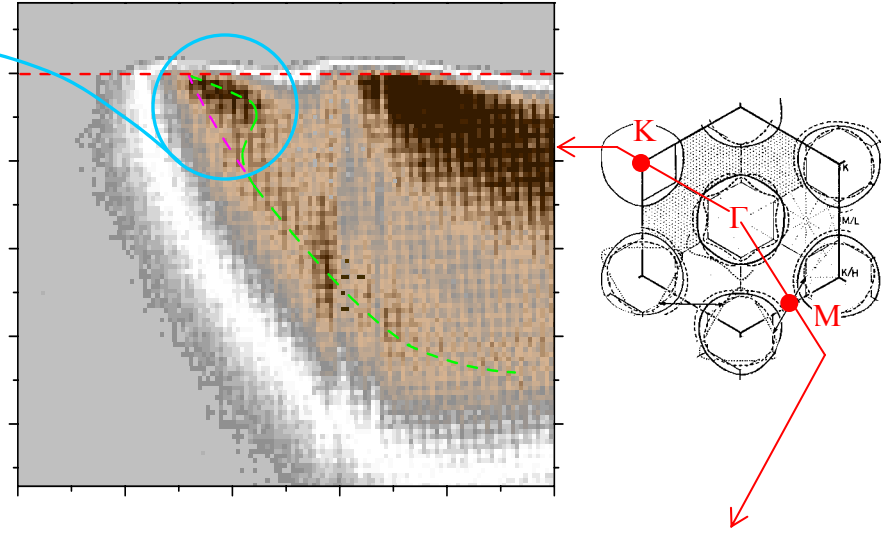
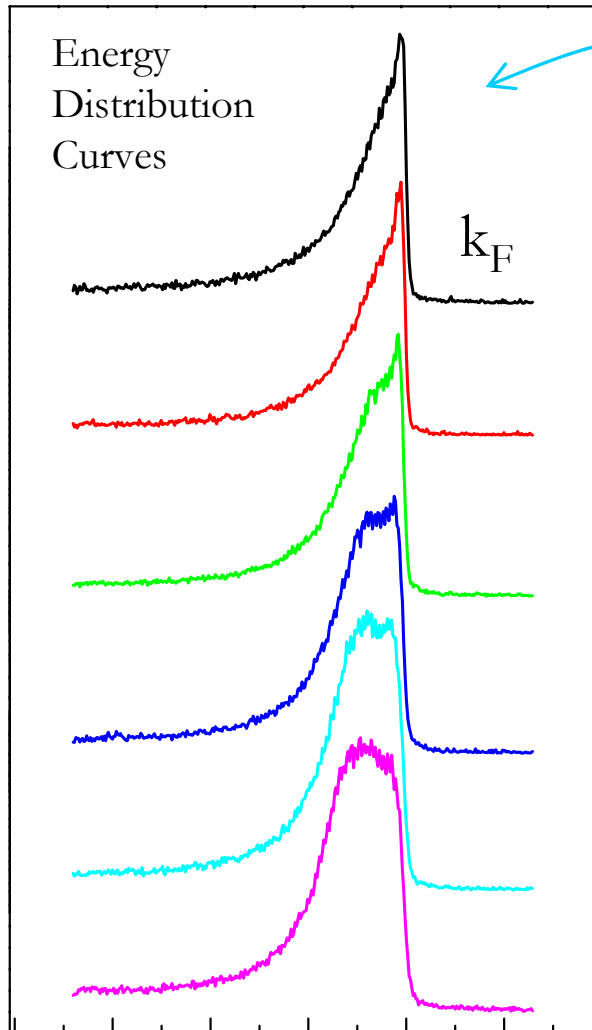
Spectral functions



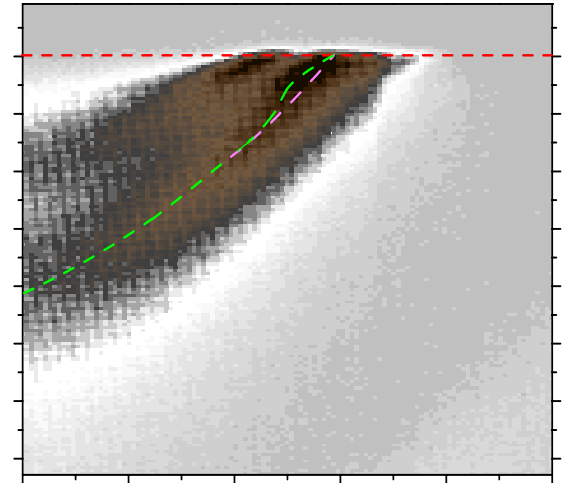
Douglas J. Scalapino
in Superconductivity,
R.D. Parks, editor

Coupling of electrons to collective modes

/phonons in a conventional superconductor $2\text{H-NbSe}_2, T_c \sim 7\text{K}/$



Coupling shows up as a “kink” in the dispersion and “peak-dip-hump” structure in EDC



★ Note a well resolved bi-layer splitting

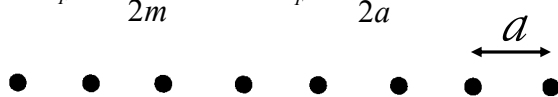
Charge Density Waves

R.E. Peirls, Quantum Theory of Solids (Clarendon, Oxford, 1955); H. Fröhlich, Proc. R. Soc. Lond. A 223, 296 (1954);
A.W. Overhauser, Phys. Rev. 167, 691 (1968); S.-K. Chan and V. Heine, J. Phys. F 3, 795 (1973)

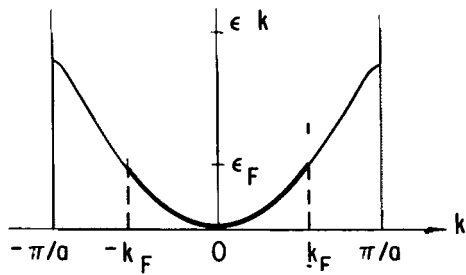
★ G. Grüner, Density Waves in Solids (Addison-Wesley, Reading, 1994) ★

1. Lets take one-dimensional electron gas...

$$\epsilon(k) = \eta^2 k^2 / 2m$$

$$\epsilon_F = \frac{\eta^2 k_F^2}{2m} \quad k_F = \frac{N_0 \pi}{2a}$$


The diagram shows a series of black dots representing lattice sites, with a double-headed arrow above them labeled 'a' indicating the lattice constant. Below the dots is a parabolic energy band structure plot. The vertical axis is labeled 'ε k' and the horizontal axis is labeled 'k'. The parabola has its minimum at k=0, ε=0. The Fermi energy ε_F is marked on the vertical axis, and the corresponding Fermi wavevector k_F is marked on the horizontal axis. The Brillouin zone boundaries are at k = ±π/a. Vertical dashed lines connect the Fermi energy level to the parabolic band at k = ±k_F.



2. Consider response of an electron gas to a time independent potential:

$$\phi(r) = \sum_q \phi(q) e^{iqr}$$

3. Rearrangement of the charge density:

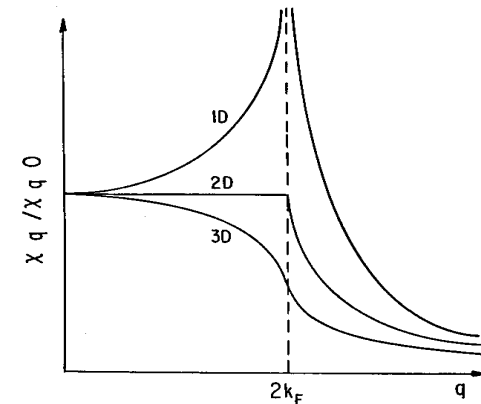
$$\rho^{ind}(q) = \chi(q) \phi(q)$$

4. χ(q)–Lindhard response function:

$$\chi(q) = \int dk \frac{f_k - f_{k+q}}{(2\pi)^d \epsilon_k - \epsilon_{k+q}}$$

In one dimension:

$$\chi(q) = \frac{-e^2}{\pi \eta v_F} \ln \left| \frac{q + 2k_F}{q - 2k_F} \right|$$



χ(q) diverges at q=2k_F

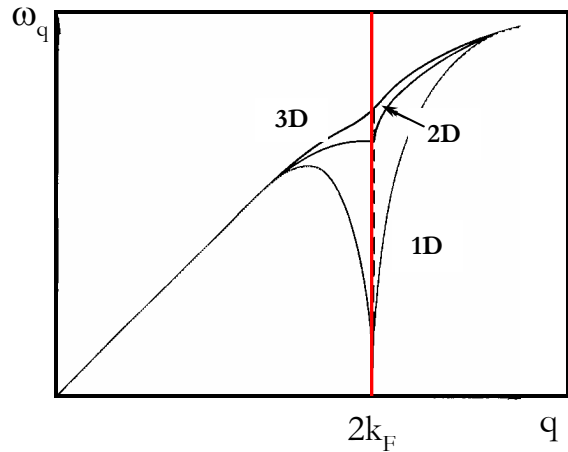


One-dimensional gas is unstable with respect to the formation of a periodically varying electron charge density

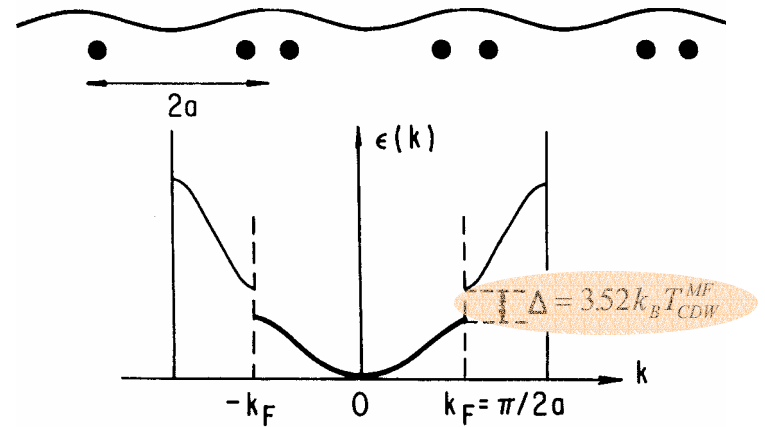
Consequences of charge modulation

/and electron-phonon coupling/

Modification of phonon spectrum
/Kohn anomaly or phonon softening at $2k_F$ /

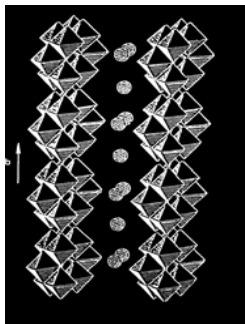


Periodic lattice modulation
and Piers transition /opening of a gap at k_F /

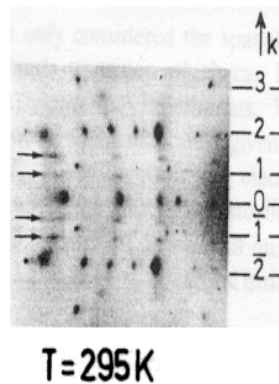


CDW in a real system: $K_{0.3}MoO_4$

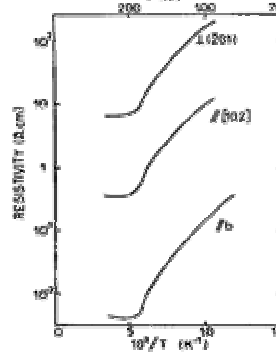
Quasi-one-dimensional
crystal structure



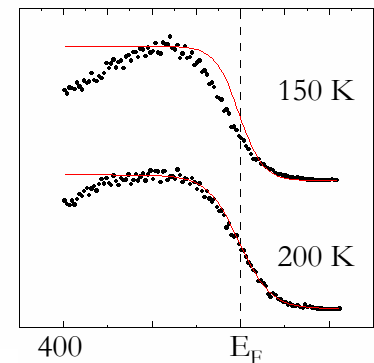
X-ray scattering



Resistivity



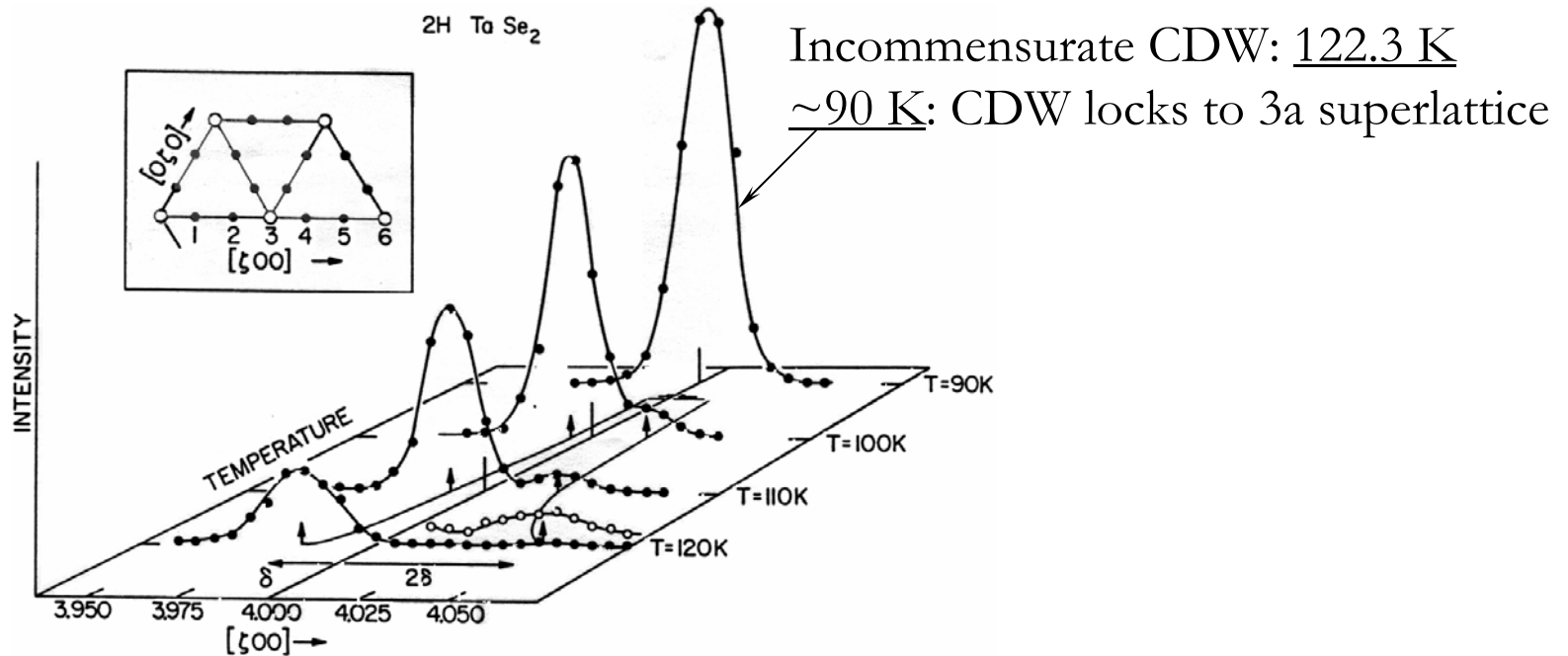
ARPES spectra at k_F



Neutron scattering experiment

/superlattice due to the Charge Density Wave/

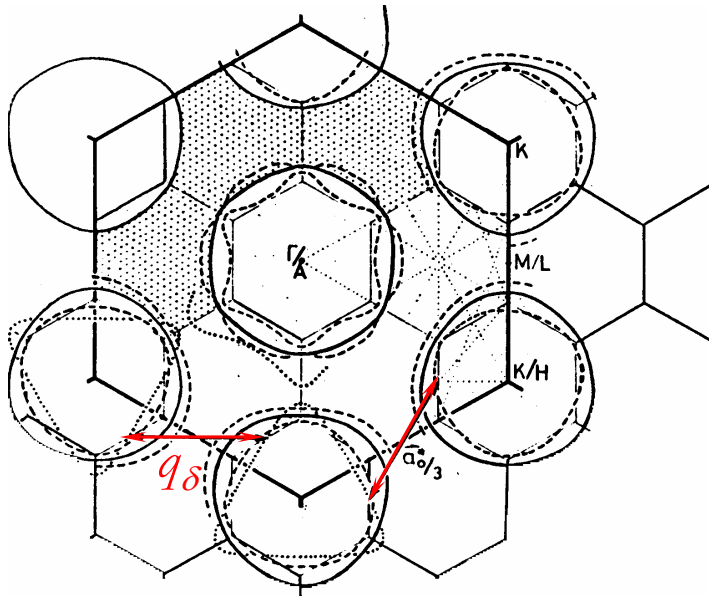
D.E. Moncton, J.D. Axe, and F.J. DiSalvo, PRL 34, 734 (1975)



$$\text{CDW wave vector: } q_{\delta} = 4\pi \{1 - \delta(T)\} / a\sqrt{3}$$

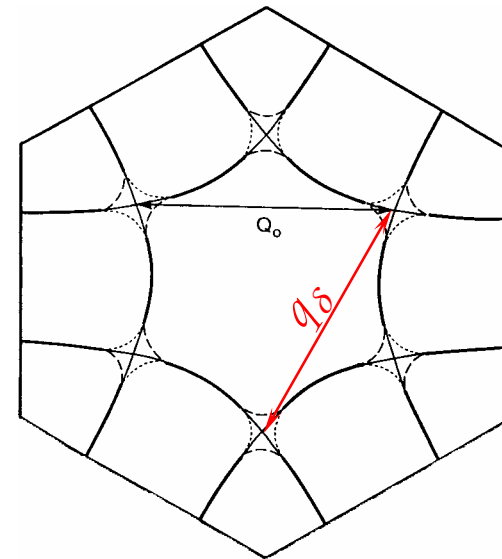
Nesting

A. Fermi surface nesting



J.A. Wilson, PRB 15, 5748 (1977)
G. Wexler and A.M. Wooley, J. Phys. C 9, 1185 (1976)
L.F. Mattheiss, PRB 8, 3719 (1973)

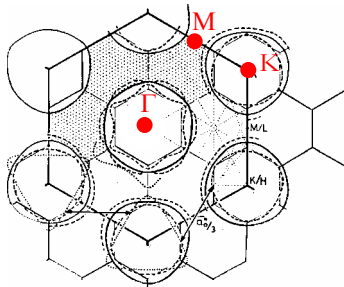
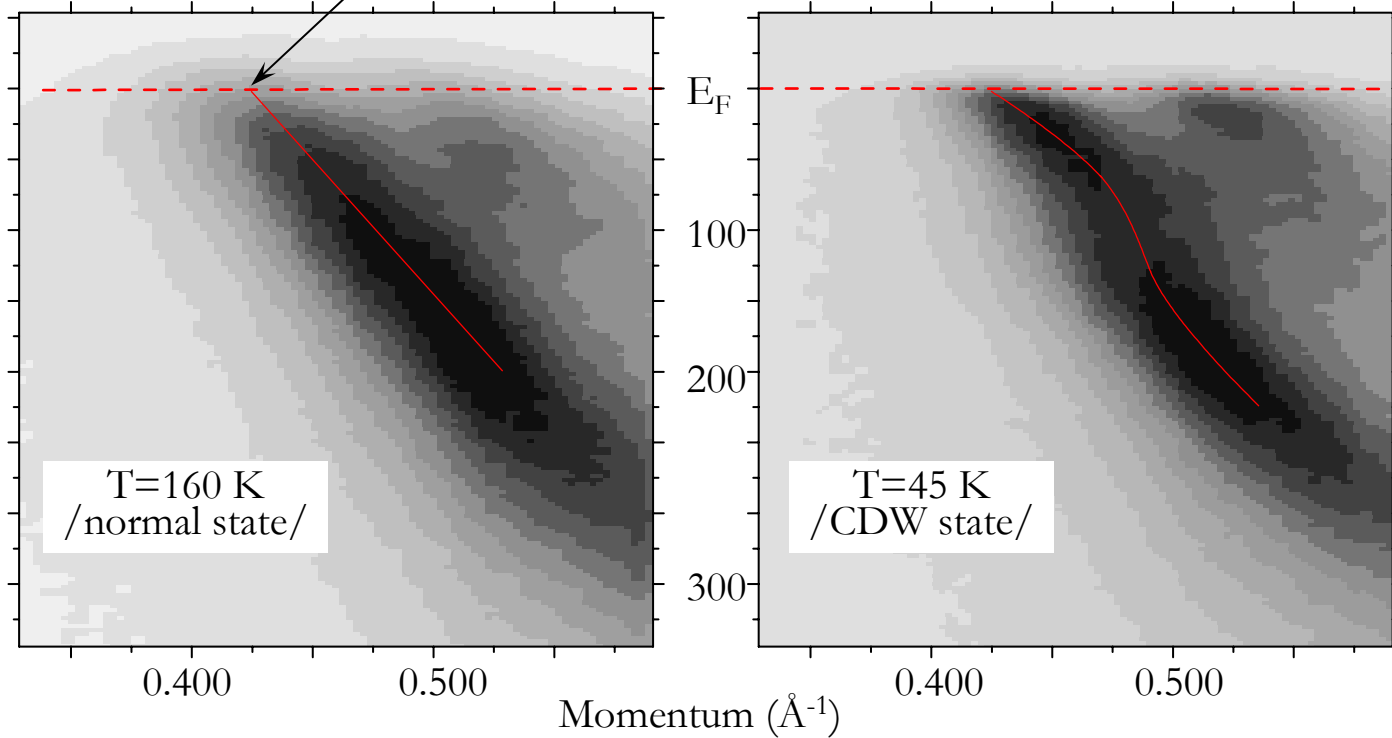
B. “Saddle point” nesting



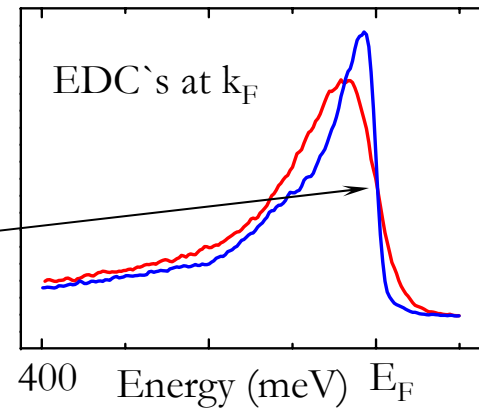
T.M. Rice and G.K. Scott, PRL 35, 120 (1975)

Band mapping along ΓM

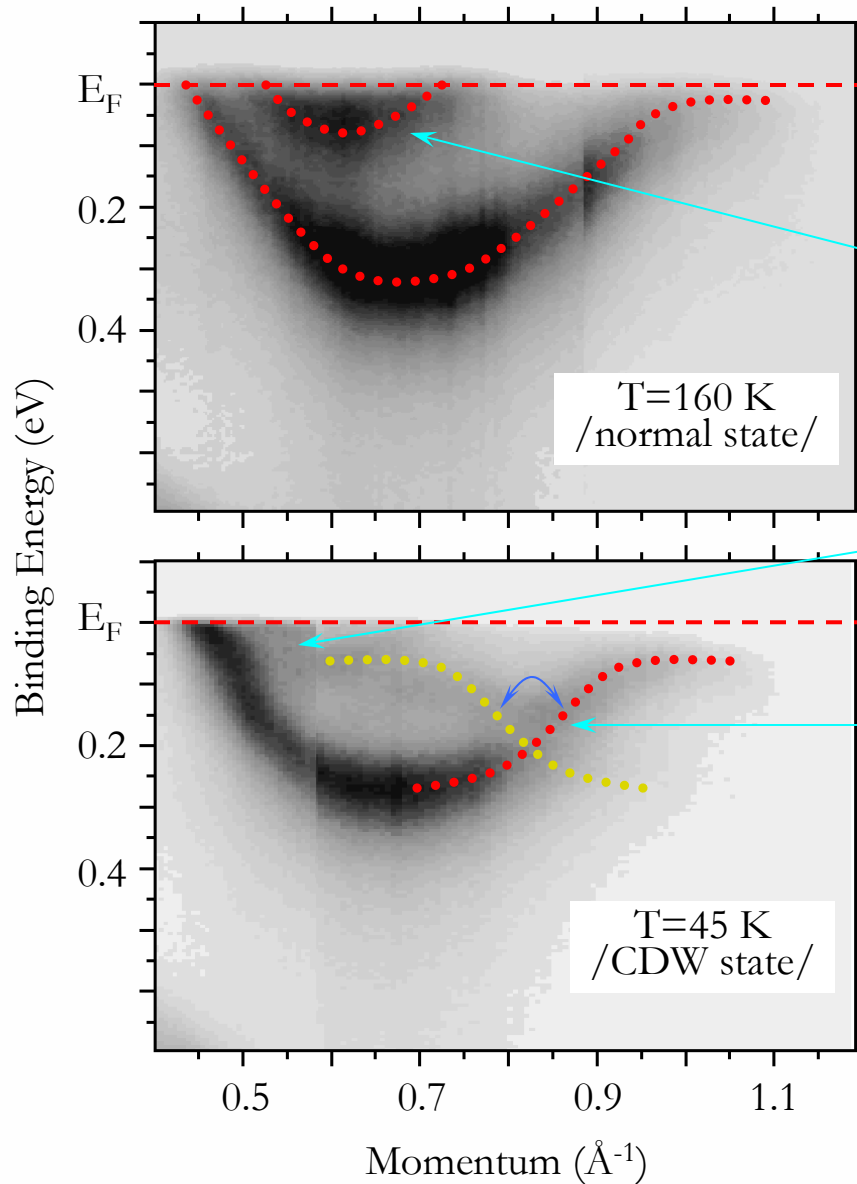
Fermi level crossing: $k_F = 0.425 \text{ \AA}^{-1}$



Nesting along ΓM is not very good and there is no gap at the Fermi level...



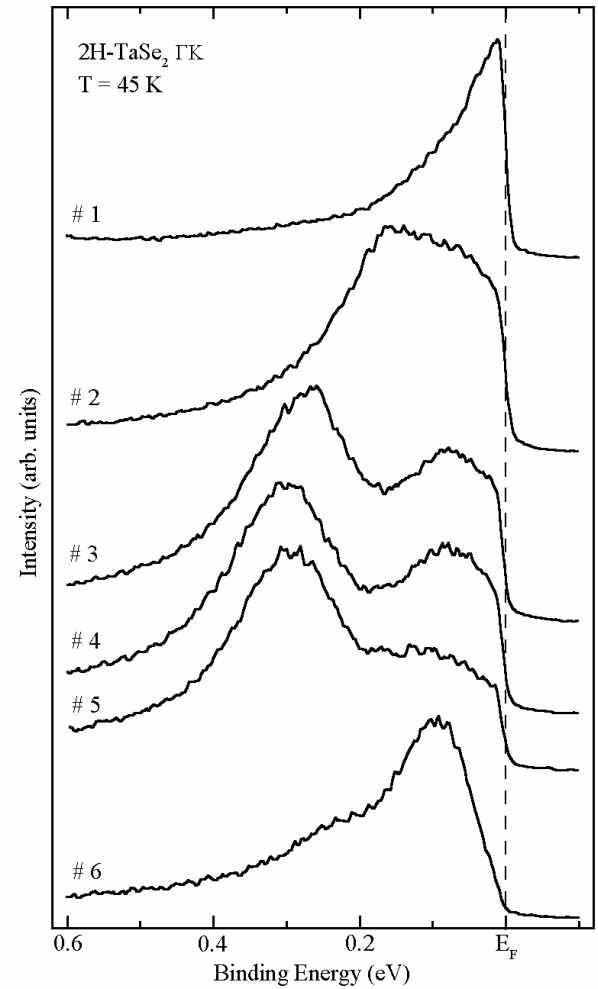
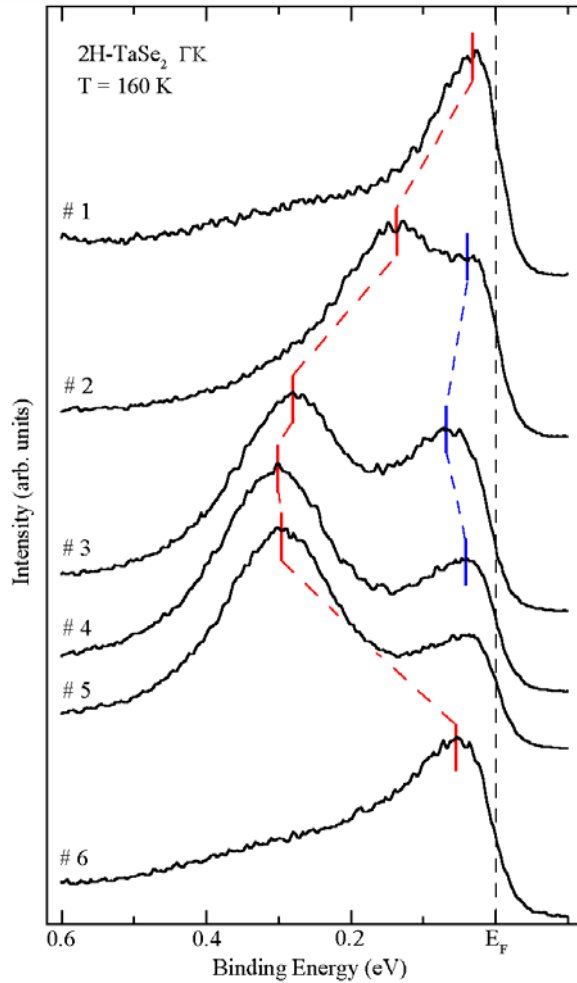
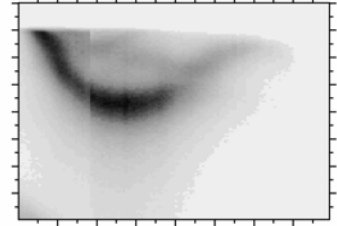
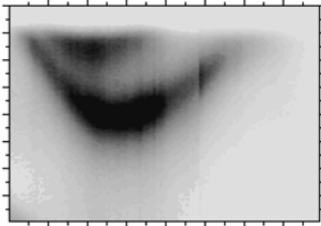
Band mapping along ΓK



New results:

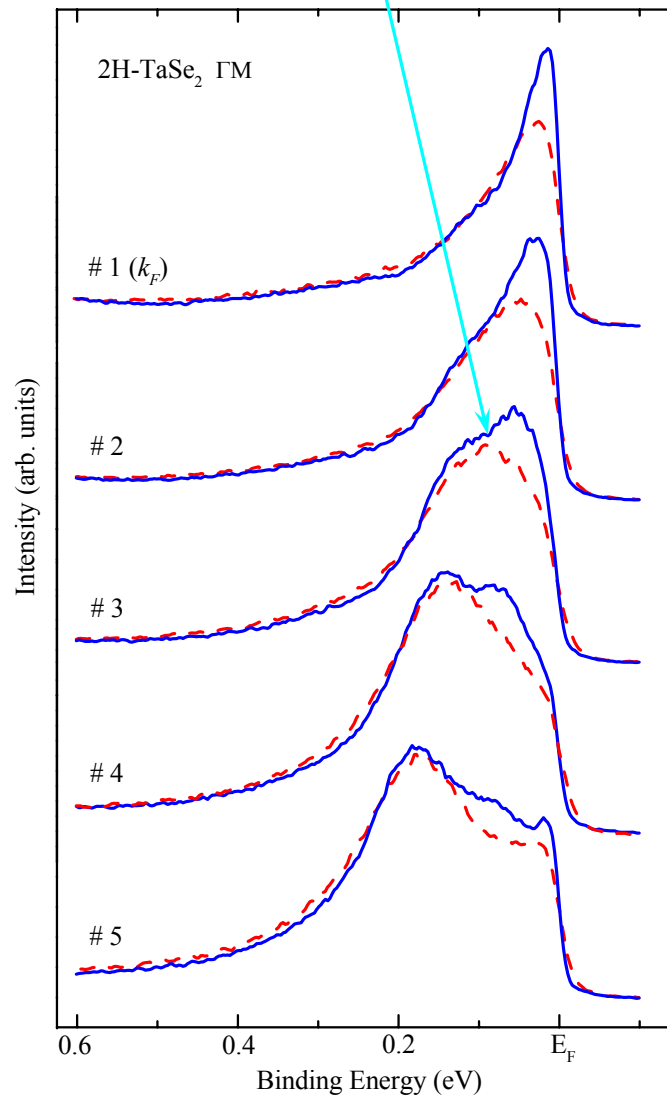
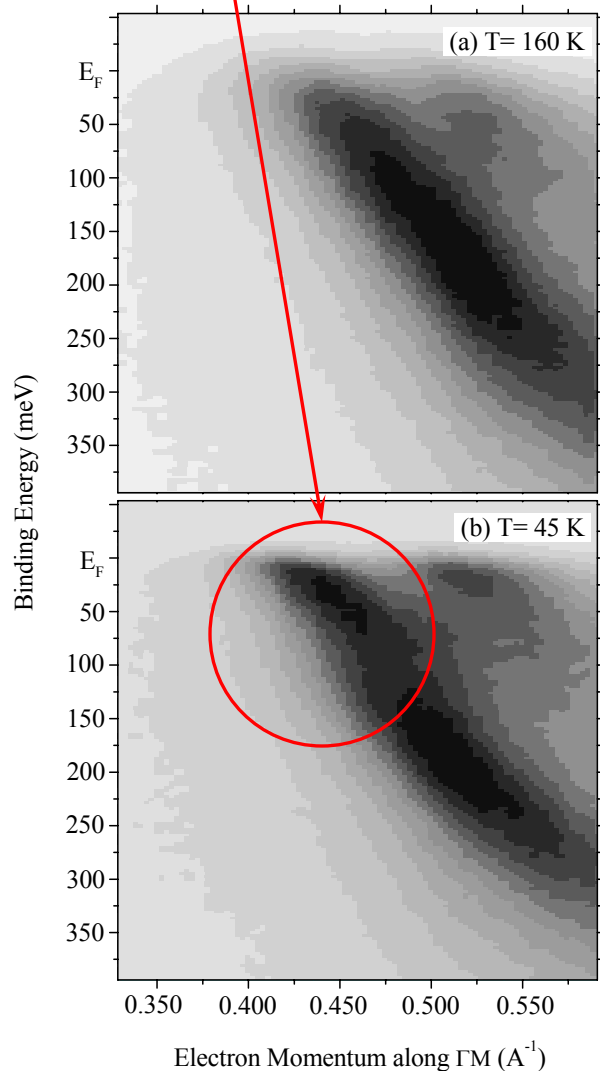
- Saddle point has a bandwidth of just ~ 50 meV and extends for only 0.2\AA^{-1}
- It is no longer there in the CDW-state
- Band “folds back” at $\sim 0.825 \text{\AA}^{-1}$; This projects into $\sim 2/3$ of ΓM

Energy distribution curves at few interesting points along Γ K



How does CDW affect low-energy excitations?

At **45 K** coupling of quasiparticles to the collective mode of some sort manifests itself via changes of both, ARPES **line-shapes** and **dispersion relations**

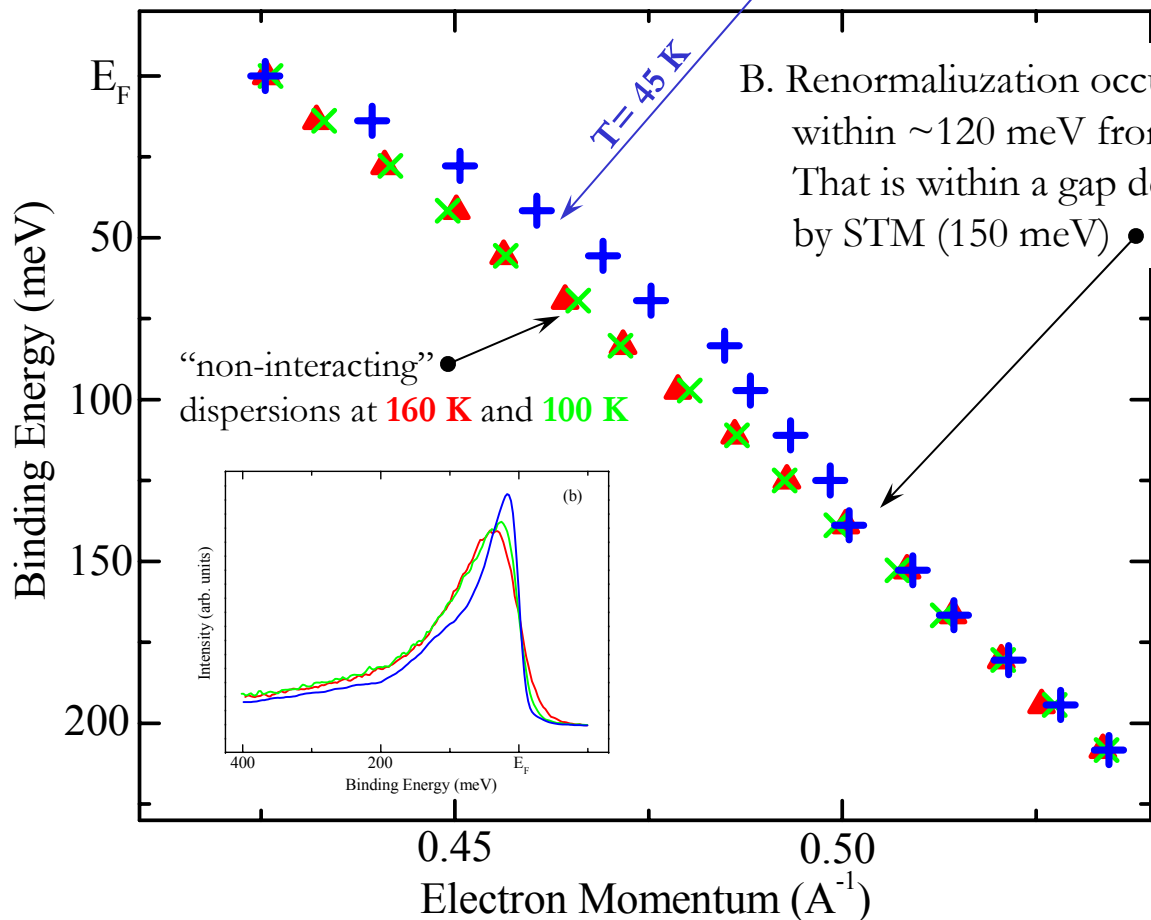


What is this collective mode?

/a few clues from dispersion relations/

A. When CDW is commensurate with the lattice

“Renormalization” of dispersion becomes obvious

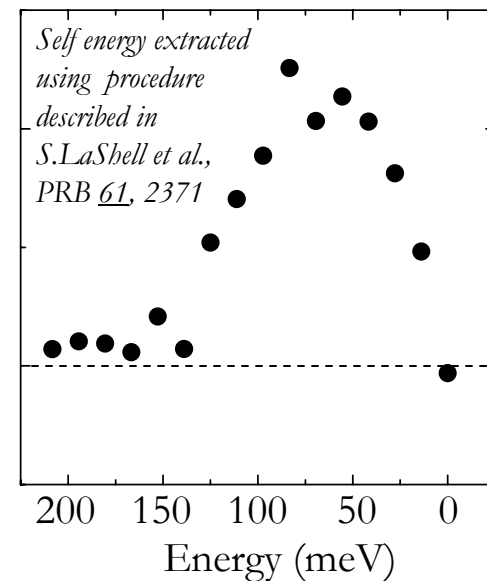


B. Renormalization occurs

within $\sim 120 \text{ meV}$ from E_F

That is within a gap detected by STM (150 meV)

C. Real part of the self energy peaks at $\sim 80 \text{ meV}$, again within a CDW gap

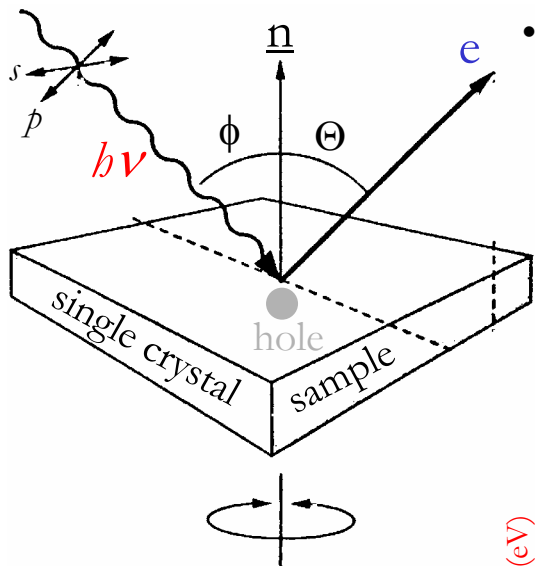


Angle Resolved Photoemission /band structure mapping/

Experiment

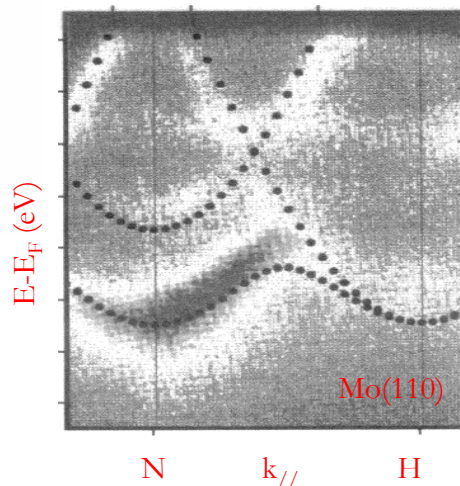
Excitation Radiation

- photon energy
- polarization
- angle of incidence



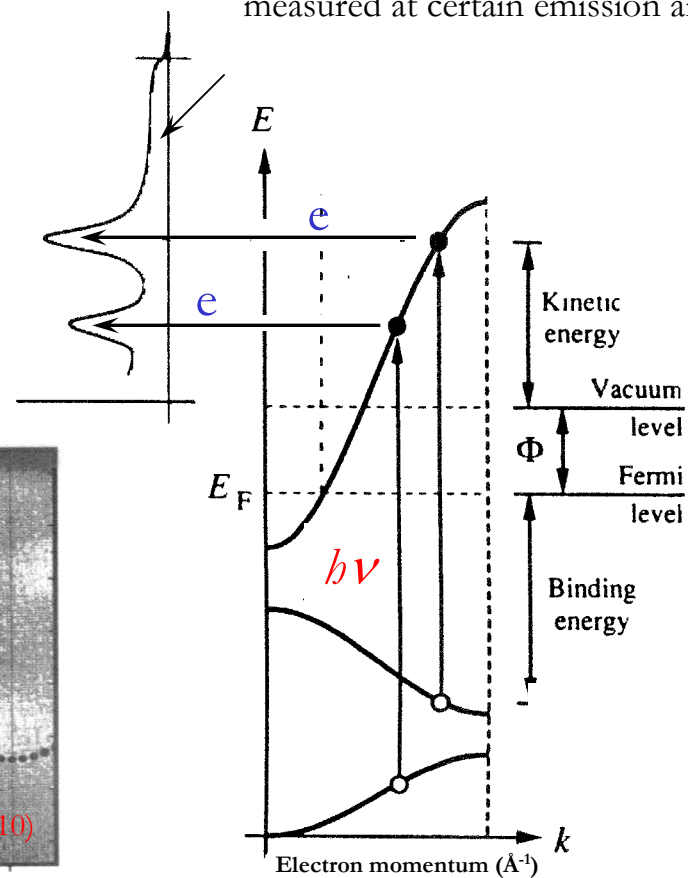
Photoelectrons

- kinetic energy
- emission angle
- polarization

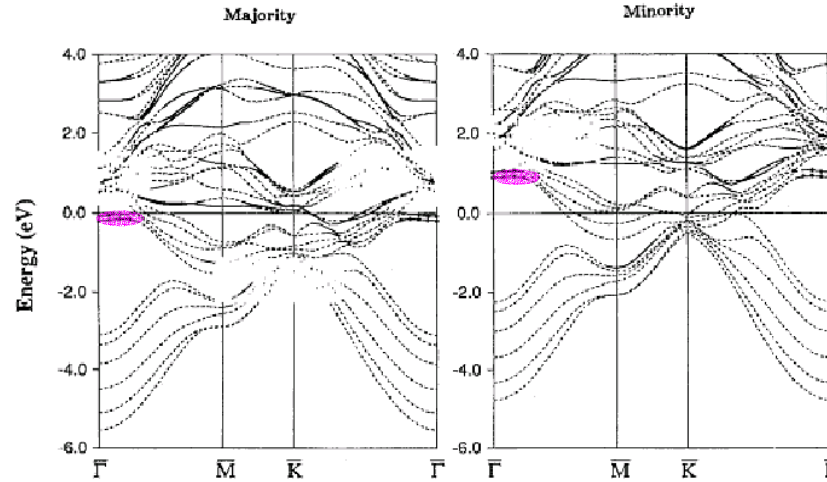


Data

Energy Distribution Curves
(photocurrent vs. kinetic energy)
measured at certain emission angle

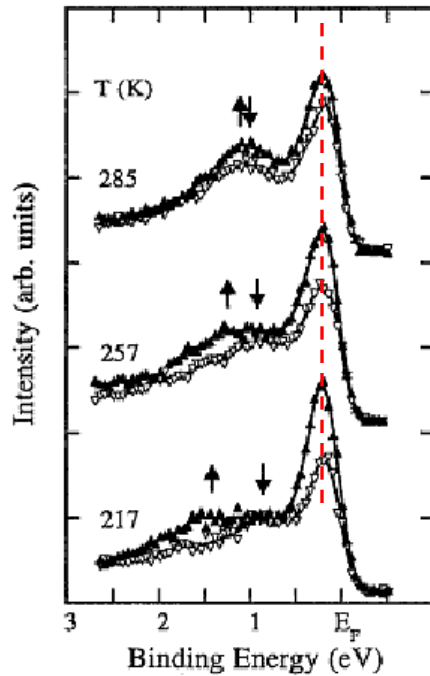


Surface state in Gd(0001)



R. Wu and
A.J. Freeman,
PRB 44, 9400

D. Li et al., PRB 51, 13895



$\Delta E \sim 175$ meV

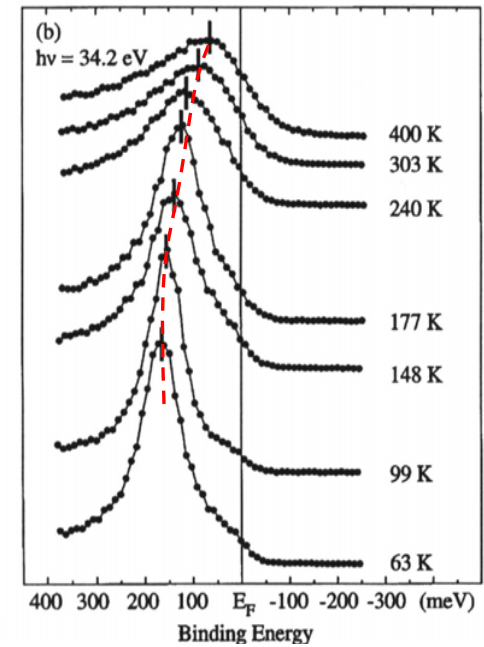
Spin-resolved

Spin-integrated

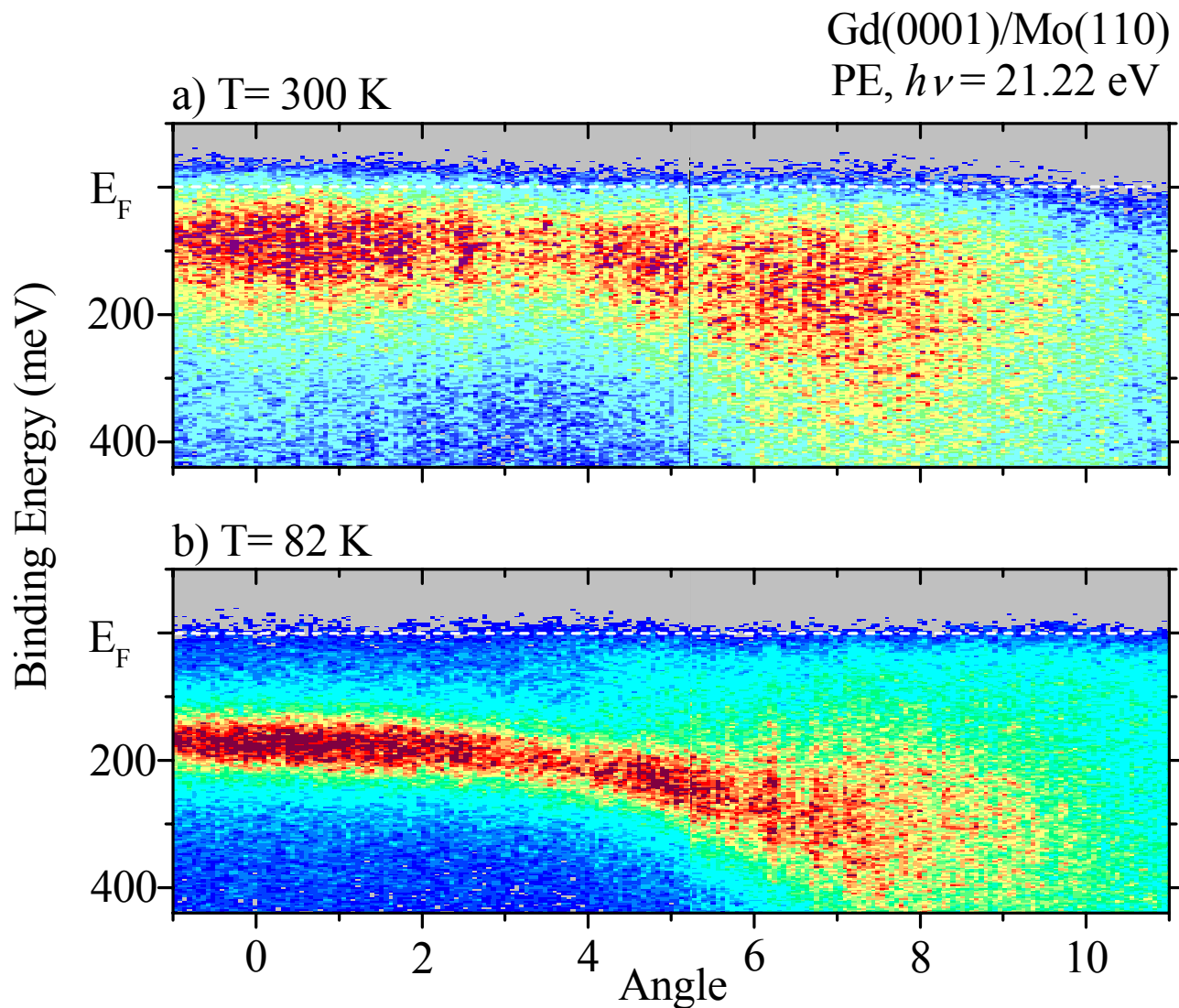
Spin-mixing

Stoner-like

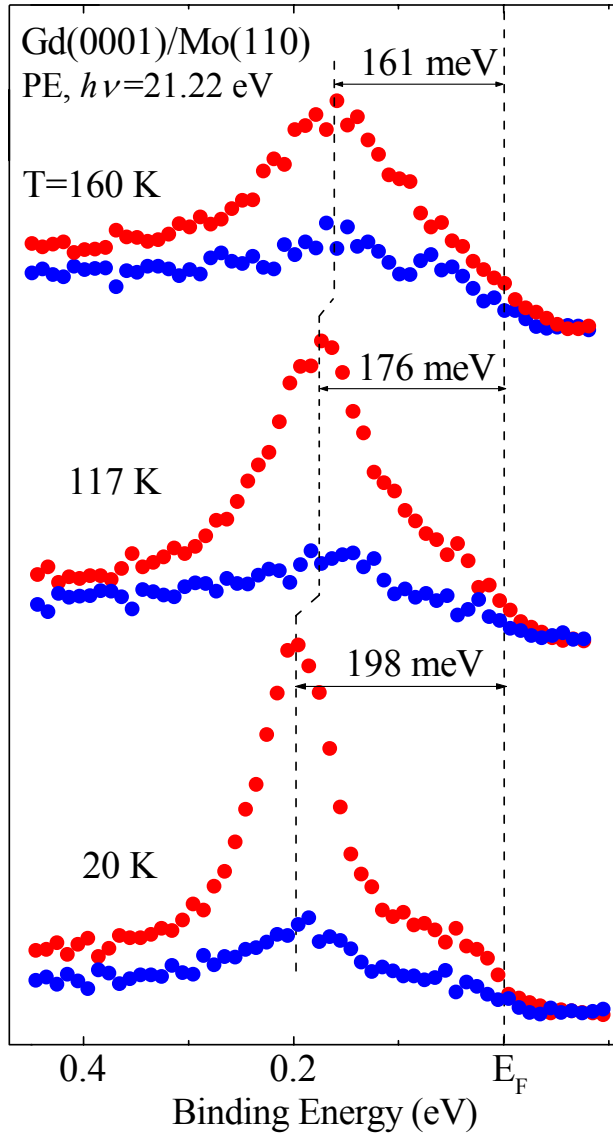
E. Weschke et al., PRL 77, 3415



Angle-resolved spin-integrated data



Spin-resolved data



Temperature-dependent shift of spin-majority peak agrees with Stoner behavior

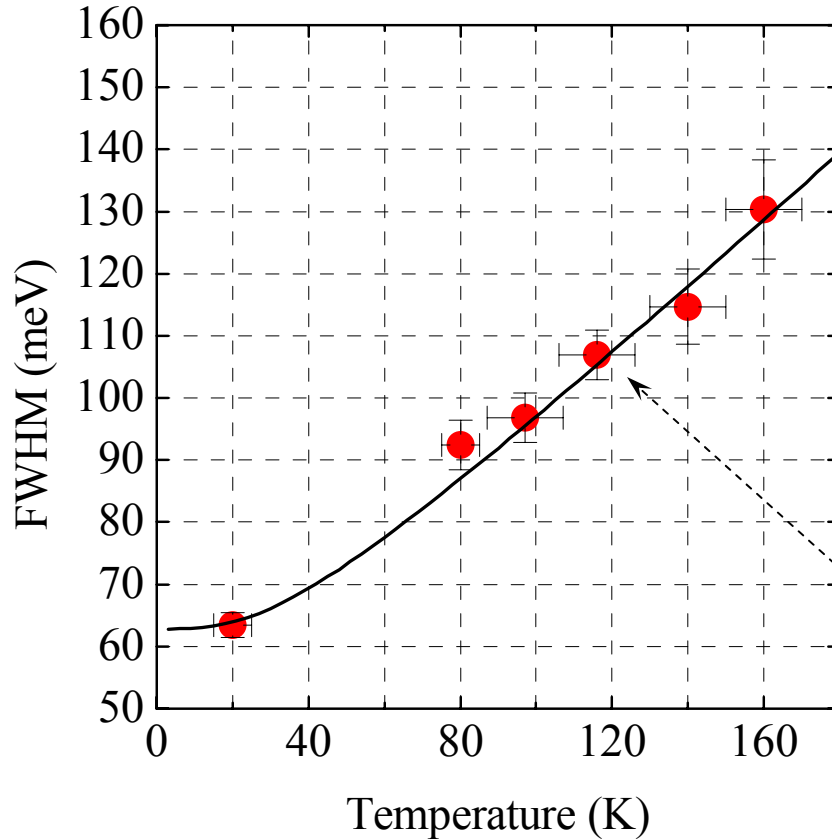
Spin-majority peak shows considerable broadening with temperature

Surface state is not 100% polarized even at 20K

Relative intensity of spin-minority component increases with temperature

Spectra were measured at six different temperatures: 20K, 80K, 98K, 117K, 140K, 160K

Width of spin-majority peak vs. temperature



Broadening of majority peak reflects mostly phonon contribution to the line-width

“Spin-resolved” electron-phonon coupling constants:
 $\lambda_{\uparrow} \sim 0.73$ $\lambda_{\downarrow} \sim 0.31$ /P. Allen/

“Spin-averaged” constant: 0.4
 /H.L. Skriver and I. Mertig, PRB **41**, 6553

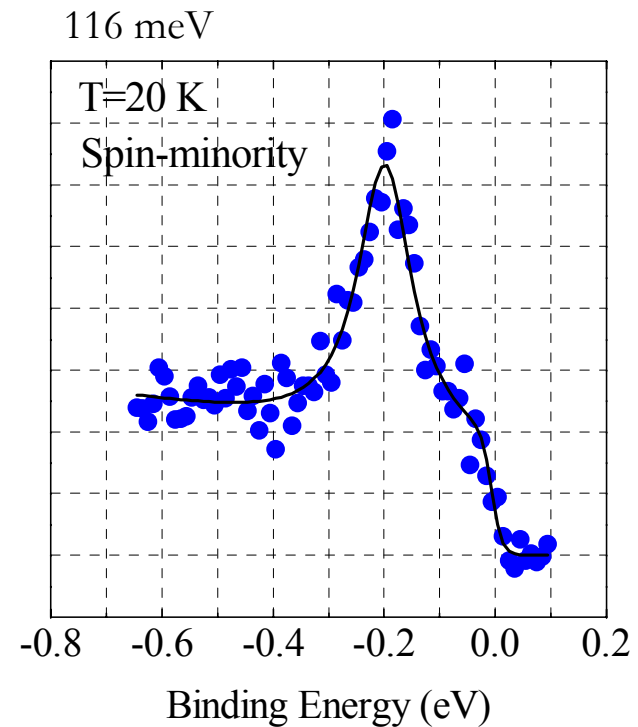
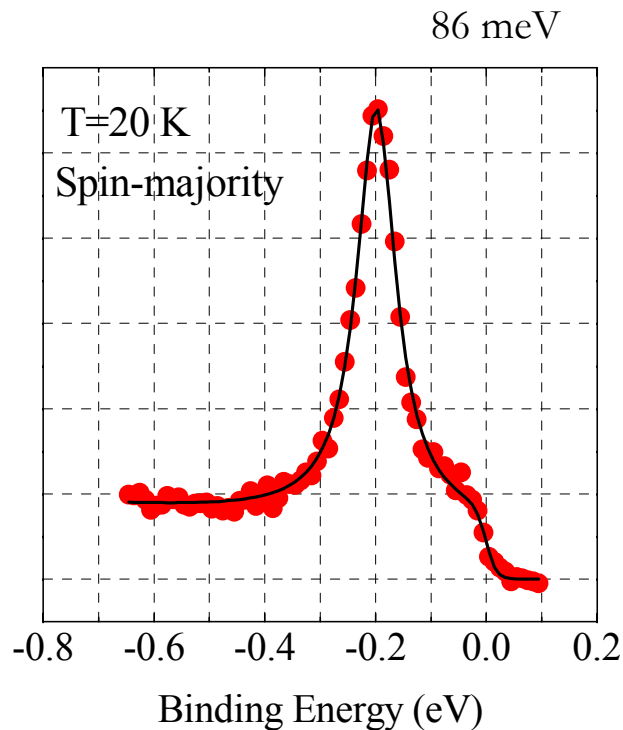
Experiment: $\lambda \sim 0.9$

$$\text{Im} \Sigma_{e-ph}(T, \omega) = \pi \int d\nu \alpha^2 F(\nu) [1 + 2n(\nu) + f(\nu + \omega) - f(\omega - \nu)]$$

Debye model: $\alpha^2 F(\omega) = \lambda \left(\frac{\omega}{\Omega_m} \right)^2$ $\frac{1}{\tau} \approx \text{const} + \pi \lambda k_B T$

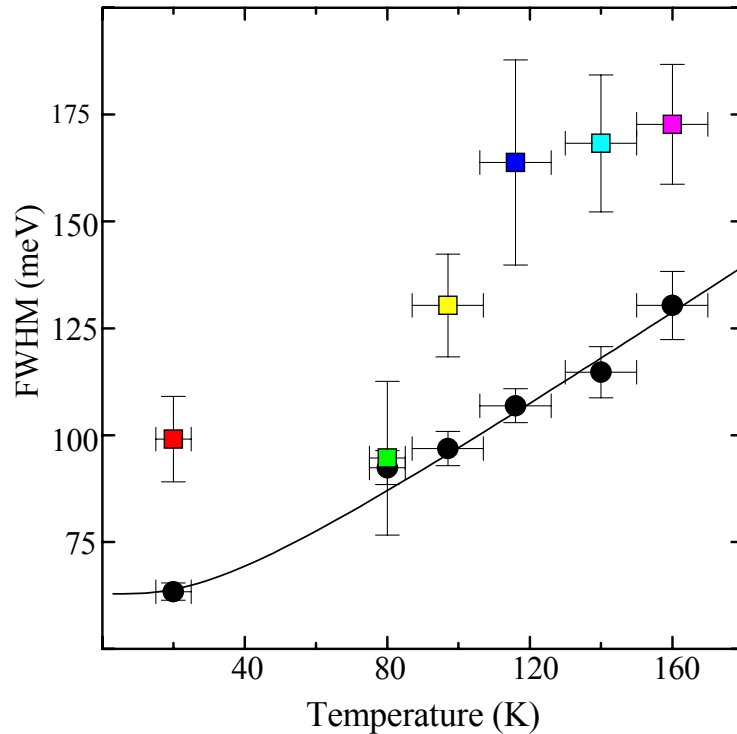
Extra broadening of spin-minority peak was detected at all temperatures

Least-square fits to Lorentzian + Fermi edge



Intrinsic width of the peak should not depend on the orientation of magnetic moment in domains

Broader minority spin channel indicates electron-magnon mechanism



P.B. Allen, PRB **63**, 214410 (2001)

$$\frac{1}{\tau^{\downarrow}} \approx \frac{P(\uparrow)m^*}{S} \left(\frac{2JSa}{\eta} \right)^2$$

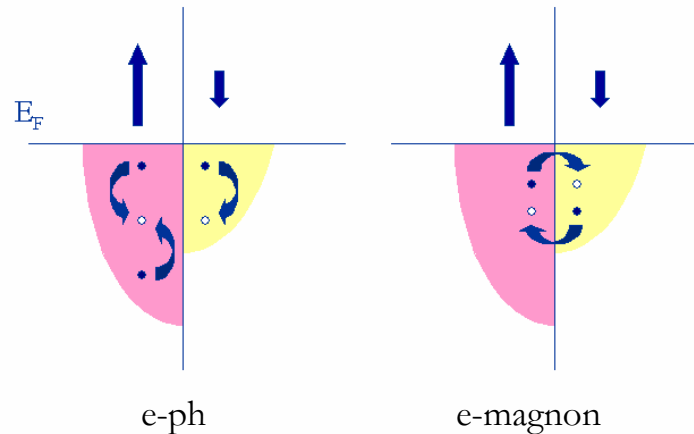


$$\frac{1}{\tau^{\downarrow}} \approx 0.095 \text{ eV}$$

$$\frac{1}{\tau^{\uparrow}} \approx 0.014 \text{ eV}$$

At low T majority spin hole decays primarily via lattice excitations, minority spin hole primarily via spin excitations

	Majority	Minority
Phonons	46 meV	10 meV
Magnons	14 meV	95 meV



History

peak-dip-hump structure at $(\pi, 0)$ is due to the coupling to the “neutron resonance”

Z.-X. Shen & J.R. Schrieffer
PRL 78, 1771 (1997)

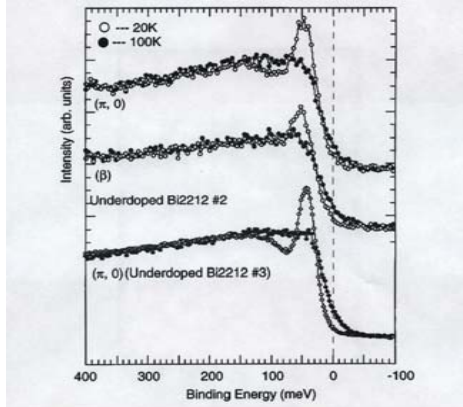


FIG. 2. ARPES data from normal and superconducting states of underdoped Bi2212 near $(\pi, 0)$. As illustrated in the inset of Fig. 1(β) is the Fermi surface crossing point along the $(\pi, 0)$ to (π, π) line and it is very close to $(\pi, 0)$. The upper two sets of curves were recorded with 35 meV energy resolution while the low set of curves was recorded with 20 meV energy resolution.

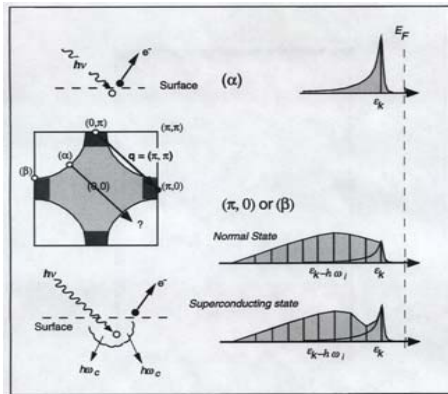


FIG. 3. Illustration of photoemission process and spectral shape in systems with weak (α) and strong couplings [β] and $(\pi, 0)$. The Fermi surface picture depicts the phase space considerations for the coupling between the quasiparticle and collective excitations near (π, π) . The light shaded area indicates the filled states, and the dark shaded area indicates the flat band region near the Fermi level.

J.C. Campuzano et al.
PRL 83, 3709 (1999)

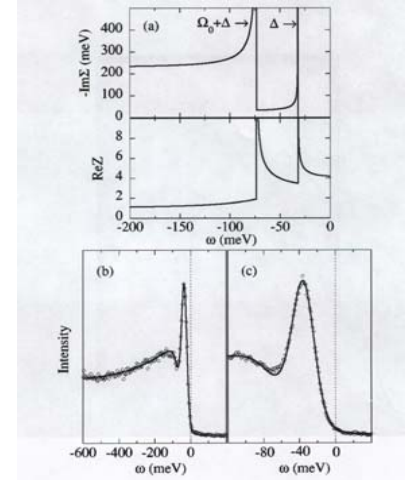


FIG. 3. (a) $\text{Im}\Sigma$ and $\text{Re}Z$ at $(\pi, 0)$ from Eqs. (2) and (3) ($\Gamma_1=200$ meV, $\Gamma_0=30$ meV, $\Delta=32$ meV, $\Omega_0=1.3\Delta$). Comparison of the data at $(\pi, 0)$ for (b) wide and (c) narrow energy scans with calculations based on Eqs. (1)–(3), with an added step edge background contribution.

M.R. Norman & H. Ding
PRB 57, R11089 (1998)

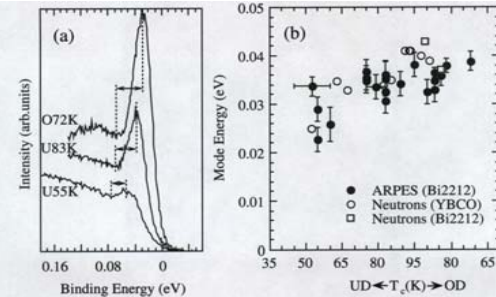


FIG. 5. Doping dependence of the mode energy: (a) Spectra at $(\pi, 0)$ showing the decrease in the energy separation of the peak and dip with underdoping. Peak and dip locations were obtained by independent polynomial fits and carefully checked for the effects of energy resolution. (b) Doping dependence of the collective mode energy inferred from ARPES together with that inferred from neutron data (for the latter, YBCO results as compiled in Ref. [5], Bi2212 results of Refs. [18] and [19]).

History

/nodal direction/

P.V. Bogdanov et al.,
PRL 85, 2581 (2000)

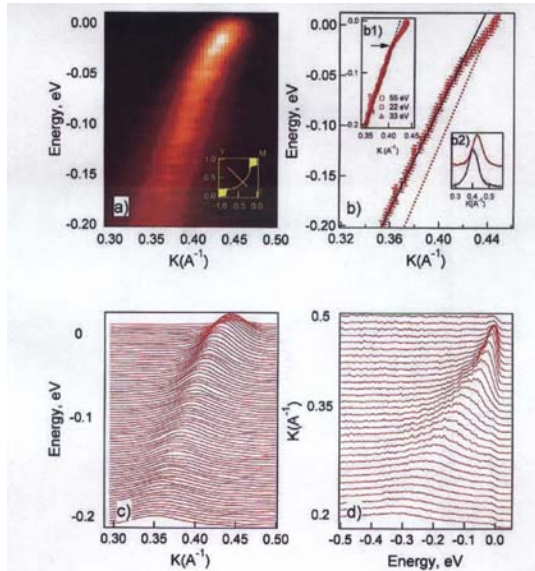


FIG. 1 (color). Panel (a) shows raw data obtained using Scienta angle mode for slightly overdoped ($T_c = 91$ K) $\text{Bi}_2\text{Sr}_2\text{CaCu}_2\text{O}_8$ along nodal direction (Γ - Y) of the BZ at 33 eV photon energy. The position of the cut is given in the inset. Panel (b) shows the dispersion of the quasiparticle determined from the MDC fits of the data in panel (a). The theoretical dispersion from LDA calculation is also included (dotted straight line). Energy is given relative to the Fermi energy. Inset (b1) shows the dispersion along this direction obtained at 22, 33, and 55 eV. Inset (b2) shows MDC's at 16 (blue) and 55 (red) meV BE. Dashed lines represent Lorentzian fits. Panels (c) and (d) show raw MDCs and EDCs, respectively.

A. Kaminski et al.,
PRL 86, 1070 (2001)

Dispersion kink
along $(0,0)$ - (π,π) is
due to the
“neutron
resonance” or
phonons...

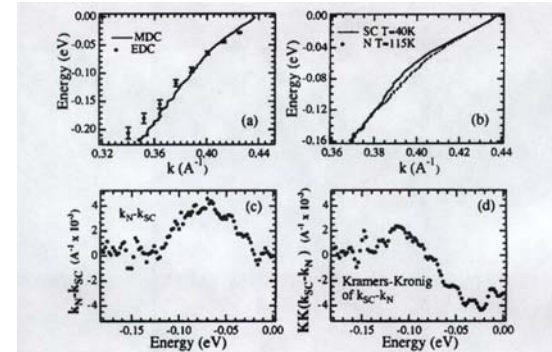


FIG. 2. ARPES data along the (π, π) direction at $h\nu = 28$ eV. (a) EDC dispersion in the normal state compared to the MDC dispersion. The EDCs are shown in Fig. 3d. (b) MDC dispersions in the superconducting state ($T = 40$ K) and normal state ($T = 115$ K). (c) Change in MDC dispersion from (b). (d) Kramers-Kronig transform of (c).

P.D. Johnson et al., PRL 87, 177007 (2001)

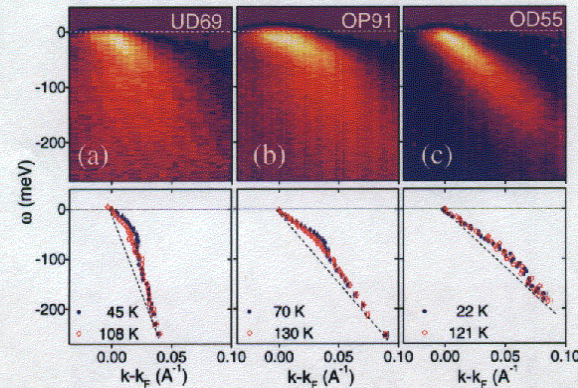


FIG. 3 (color). Upper panels: two dimensional photoemission intensities observed from (a) underdoped (UD), (b) optimally doped (OP), and (c) overdoped (OD) samples. The superconducting transition temperatures are indicated. Lower panels: the dotted lines indicate the MDC deduced dispersions for both the superconducting (blue dots) and normal states (open red diamonds) corresponding to the different samples in the panels above.

History

/theoretical work/

PDH structure at $(\pi-0)$

Kink along the node

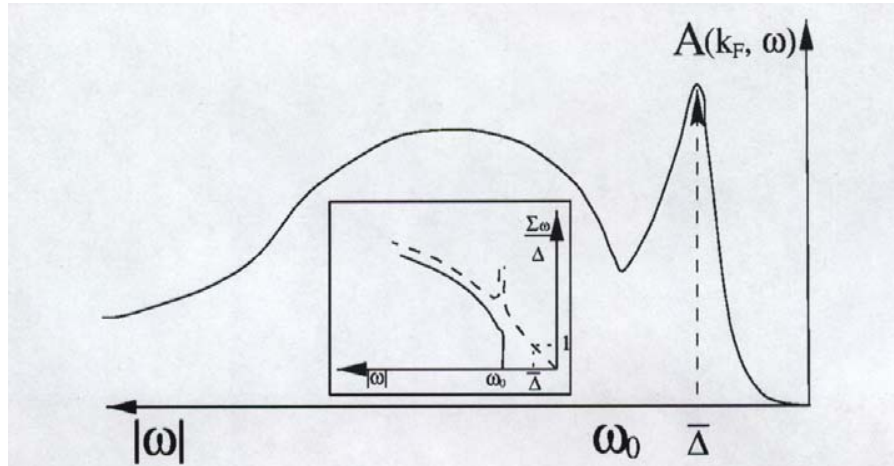


FIG. 2. Same as in Fig. 1 but at strong coupling. The resonance and onset frequencies are presented in the text. The spin resonance frequency $\Omega_{res} \propto \xi^{-1}$, is equal to the distance between the measured gap $\bar{\Delta}$ and the dip frequency ω_0 . The hump frequency differs from $\bar{\Delta}$ roughly by $\xi^{0.7}$.

Ar. Abanov & A. V. Chubukov
PRL 83, 1652 (1999)

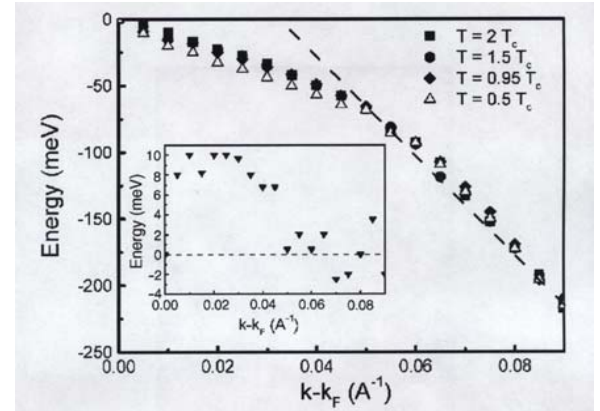


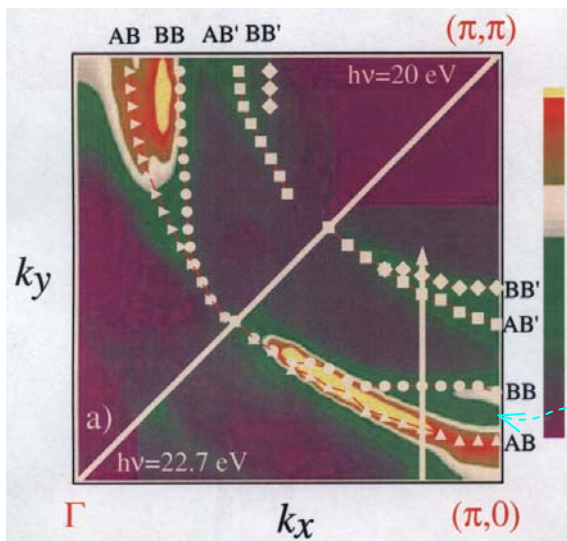
FIG. 2. Positions of the peaks in the spectral density $A(\mathbf{k}, \omega)$ versus $\mathbf{k} - \mathbf{k}_F$ (energy dispersion) along the $(0,0) \rightarrow (\pi,0)$ direction of the BZ calculated within the FLEX approximation. This has to be compared with the position of the peaks derived from the momentum distribution curve (MDC) for a hole-doped superconductor as measured in experiment. The curves show a "kink" at energies about $\hbar\omega \approx 65 \pm 15$ meV. The dashed line is a guide to the eyes. We find small changes due to superconductivity which almost coincide with the kink position. Inset: Change in the peak position in $A(\mathbf{k}, \omega)$ in the superconducting state ($T = 0.5T_c$). The results are in fair agreement with ARPES data [3].

D. Manske, I. Eremin
And K.H. Bennemann
PRL 87, 177005 (2001)

Bi-layer splitting

Recent progress in ARPES and improvements in the sample quality enabled the direct observation of bonding and anti-bonding bands in BISCO

Hence, we had a good reason to go back and look at PDH and kinks, particularly at $(\pi, 0)$, where splitting is strongest



D.L. Feng et al.,
PRL 86, 5550 (2001)

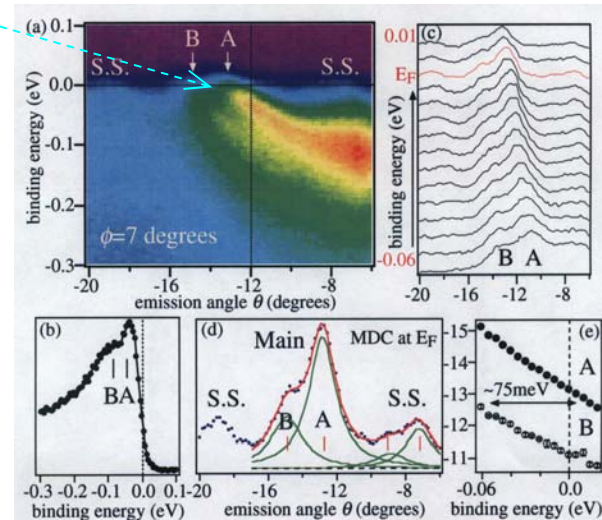


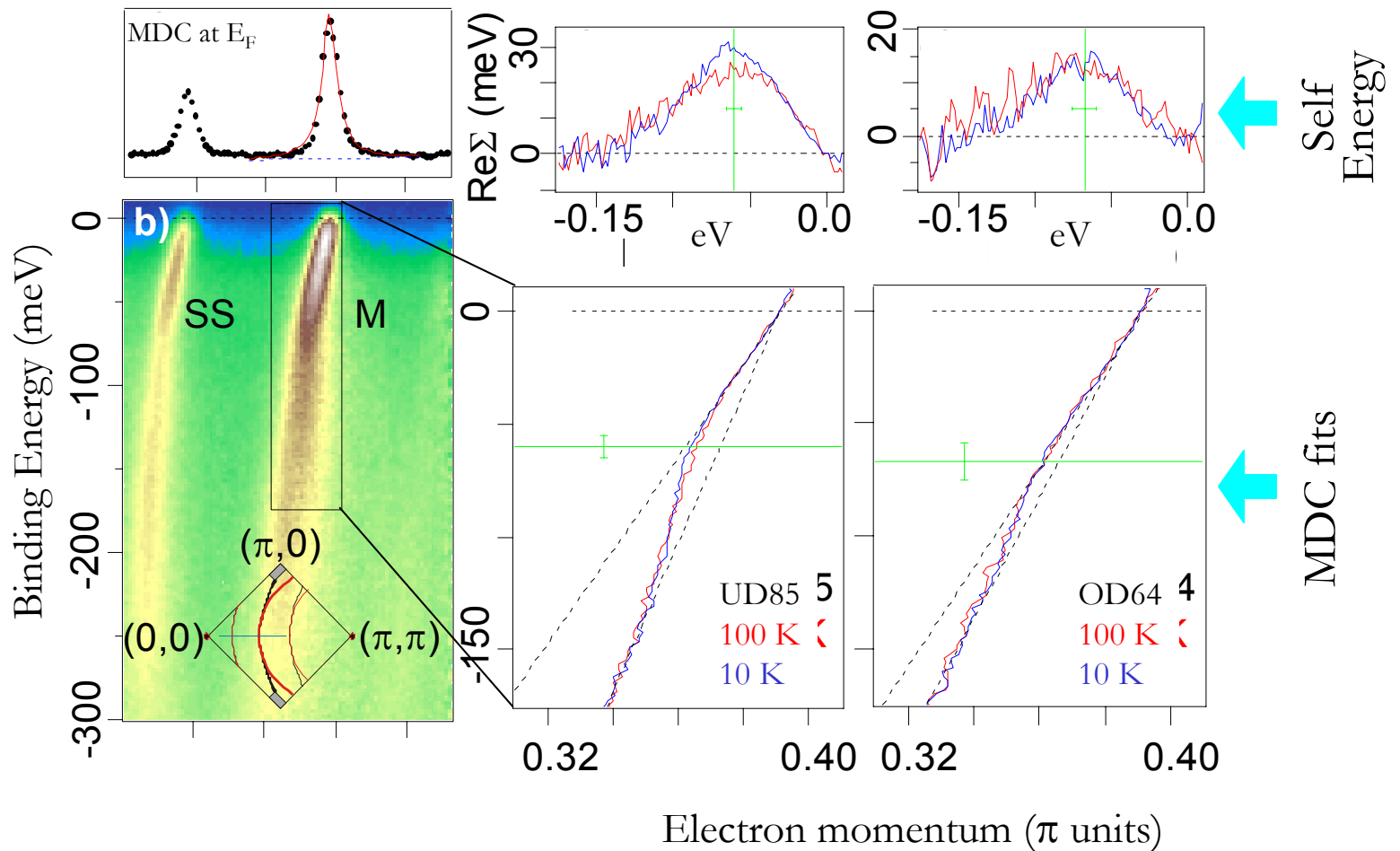
FIG. 2 (color). (a) False color plot of E vs emission angle θ for the $\phi = 7^\circ$ cut [white line in Fig. 1(a)]. (b) EDC at $\theta = -12^\circ$ from panel (a) (vertical black dashed line). Two distinct features, A and B , can be clearly seen in this EDC. (c) MDCs from panel (a) from binding energies $+10$ to -60 meV, with 5 meV steps. (d) The MDC at E_F (blue dots), including a deconvolution of the main band (red line shows the fitting result) into two Lorentzian functions A and B (green lines) plus two corresponding features in superstructure band (black dashed line). (e) The energy dependence of the θ value of MDC peaks A (closed circles) and B (open circles). The error bar from the fitting is smaller than the symbol size.

Y.-D. Chuang et al.,
PRL 87, 117002 (2001)

New
Data

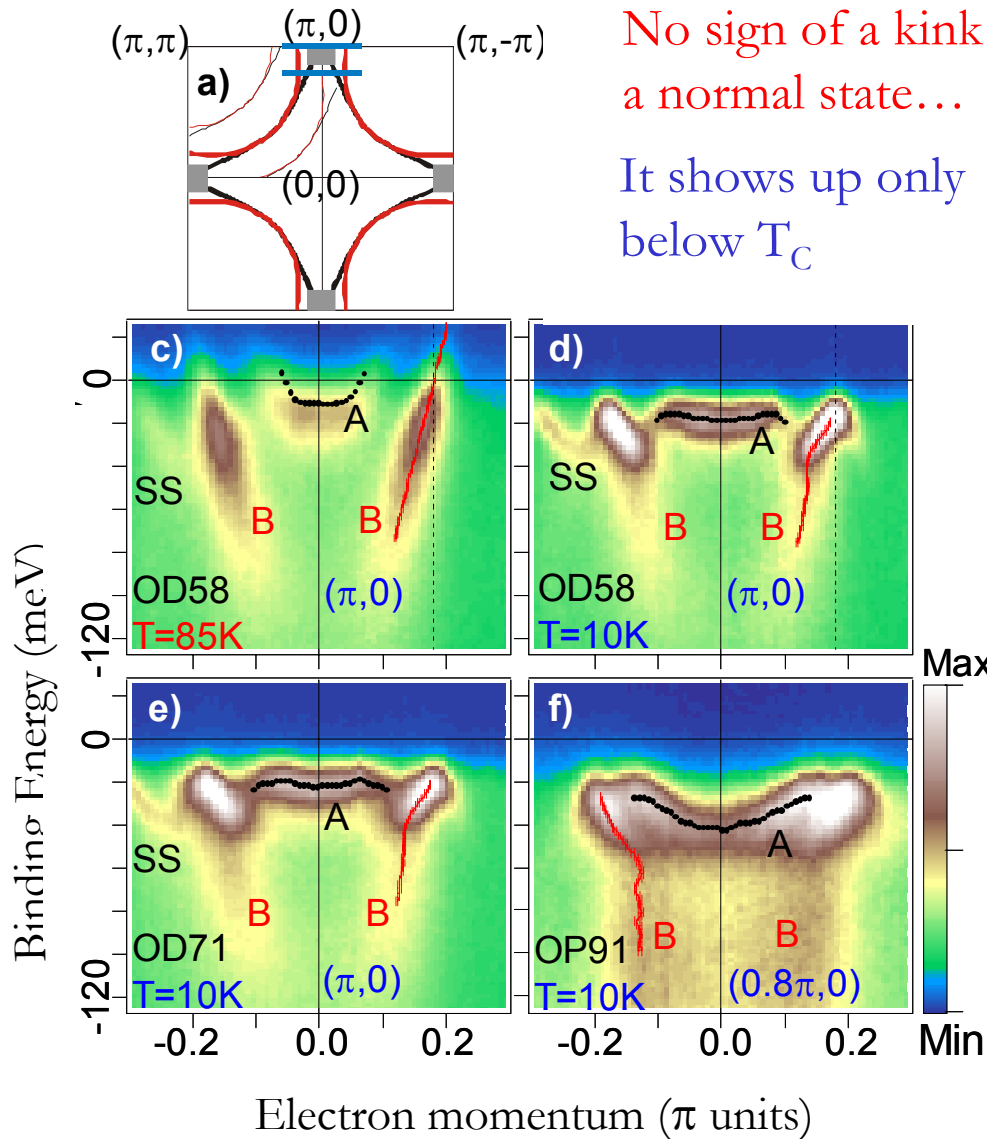
Kink along the node in underdoped and overdoped samples

Kink /S-shaped / is well—resolved above and below T_C and it does't change much at transition



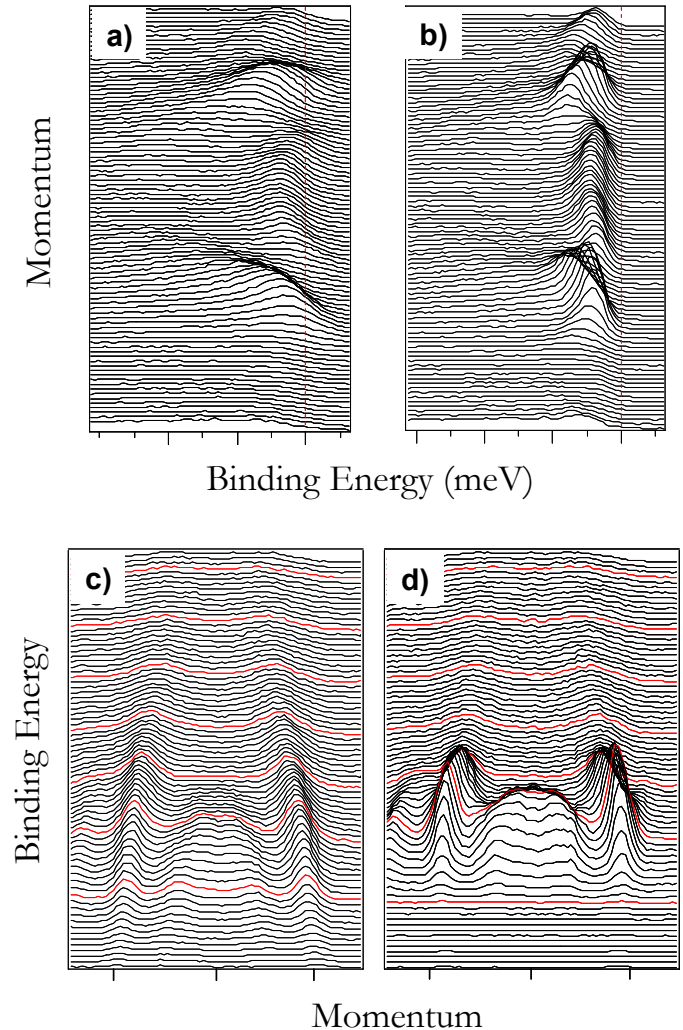
Kink at $(\pi, 0)$

bi-layer splitting and superstructure are clearly resolved

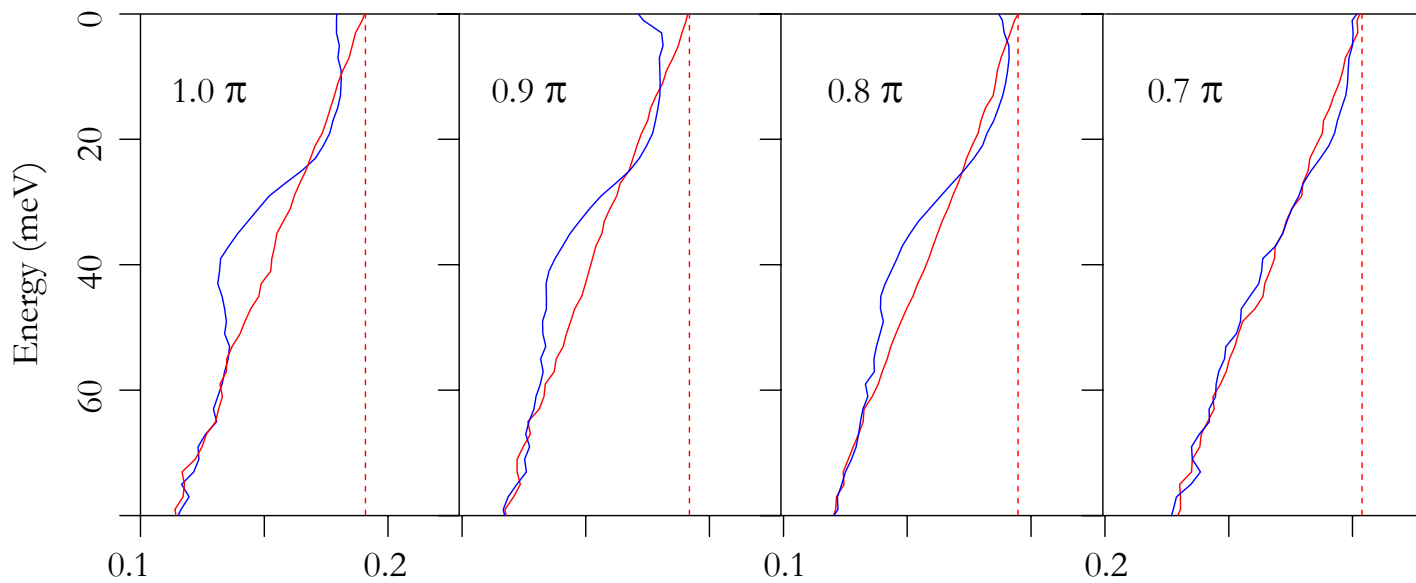
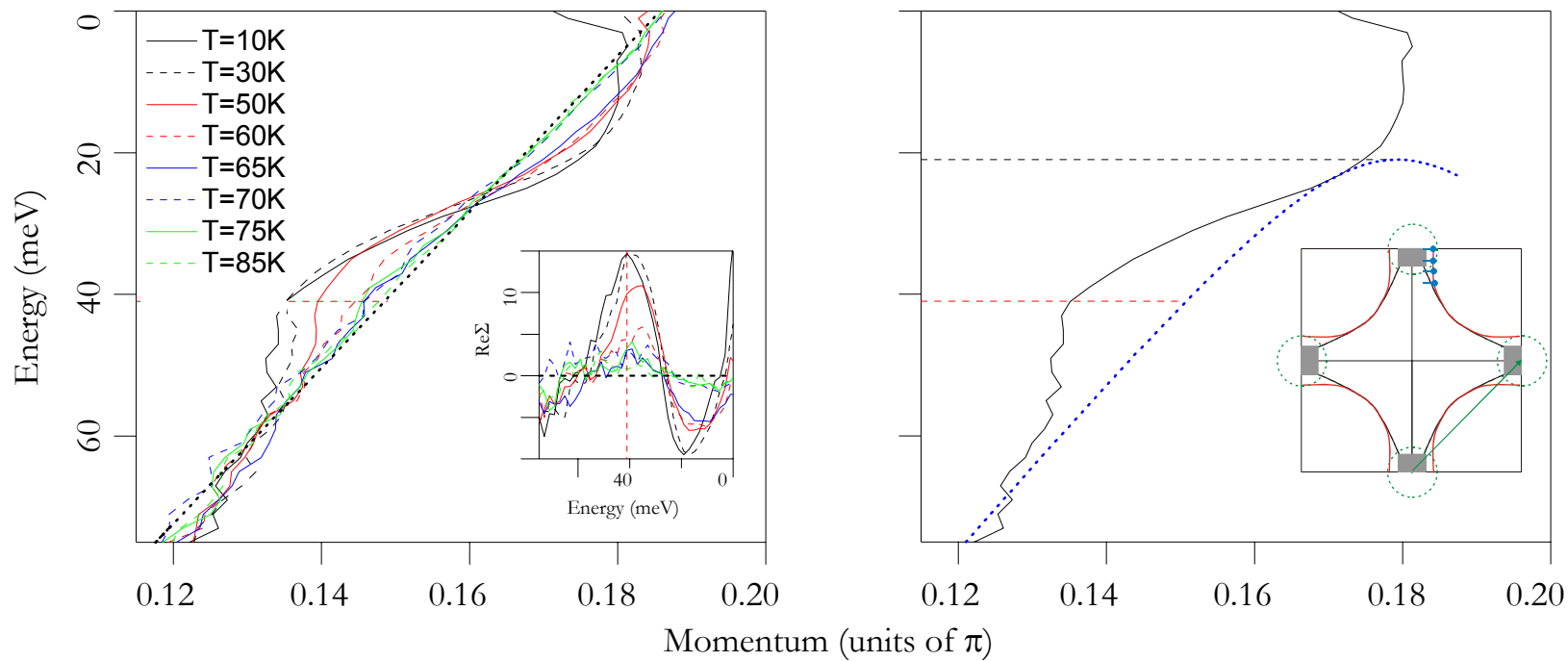


No sign of a kink in a normal state...

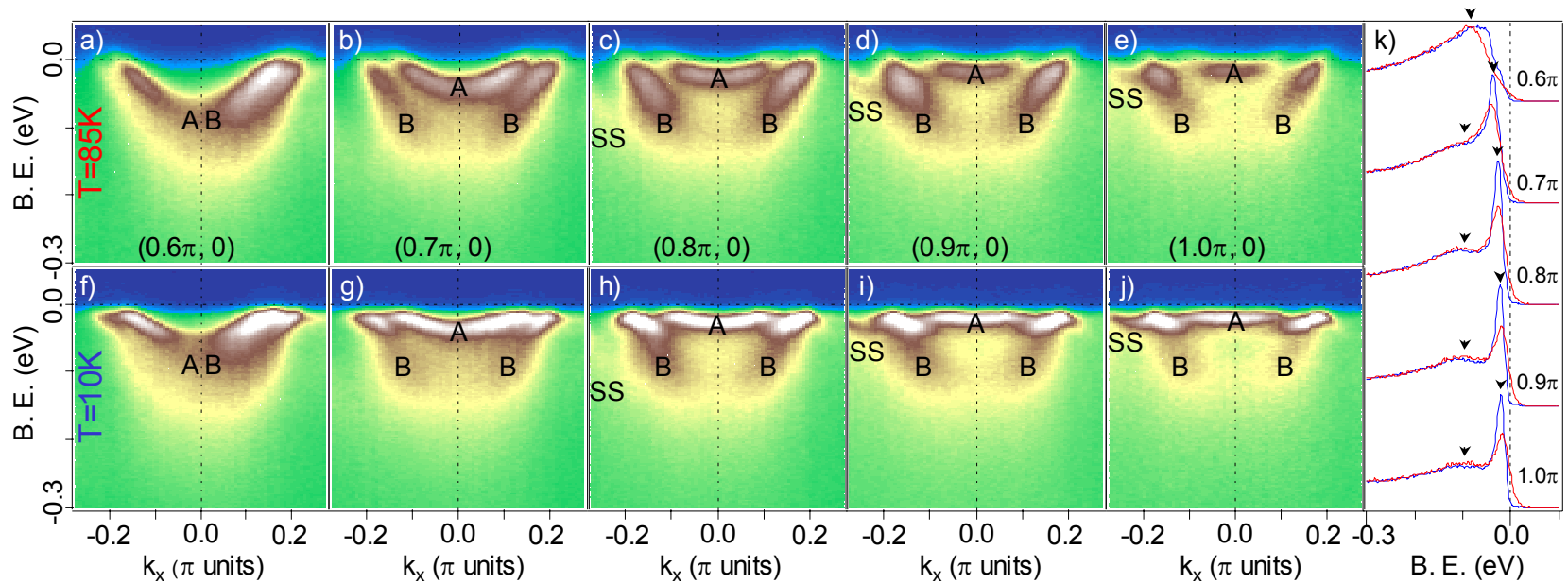
It shows up only below T_C



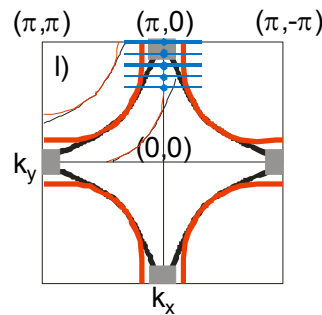
Temperature and Momentum Dependence, $(\pi;0)$



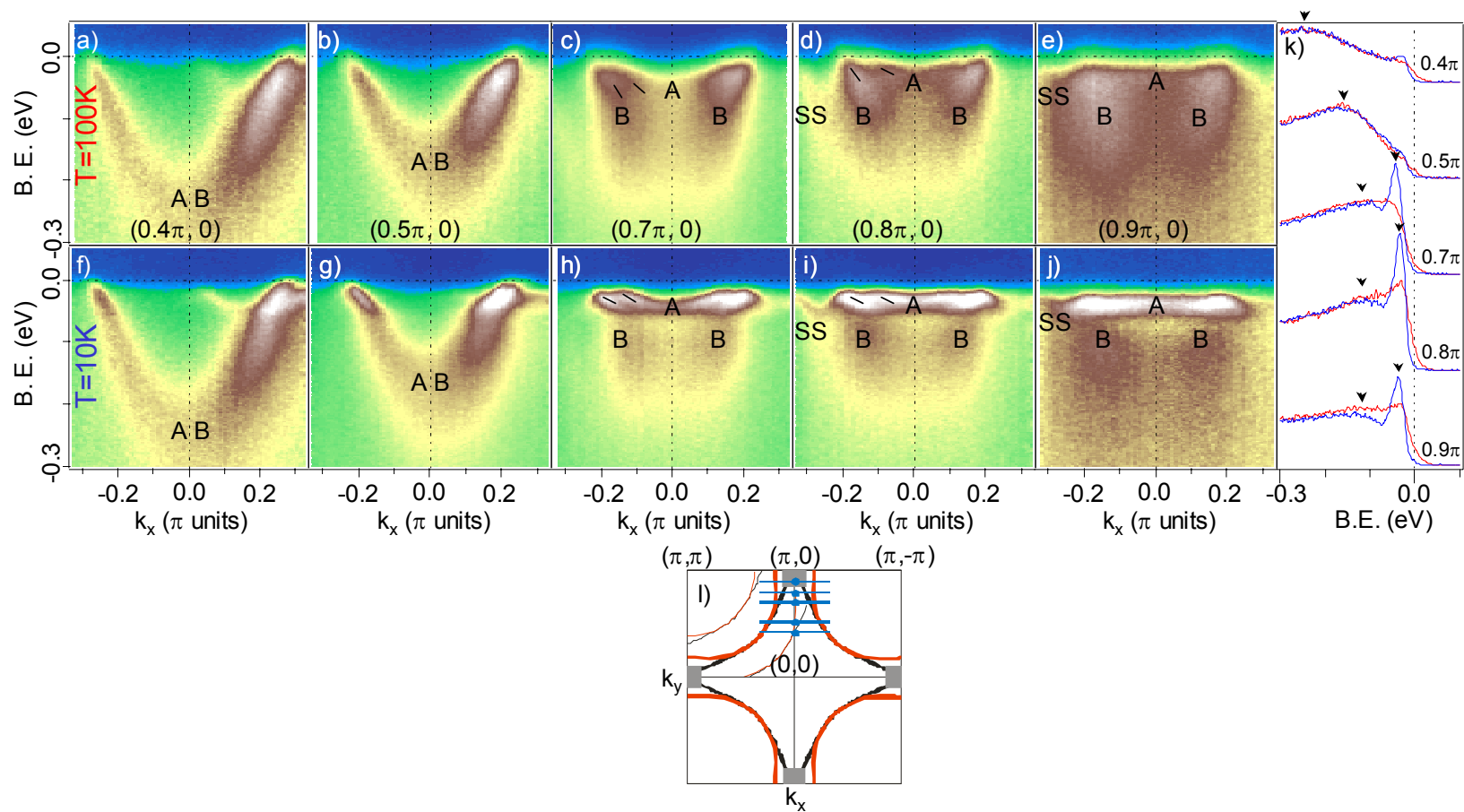
Overdoped sample, $T_C = 71$ K



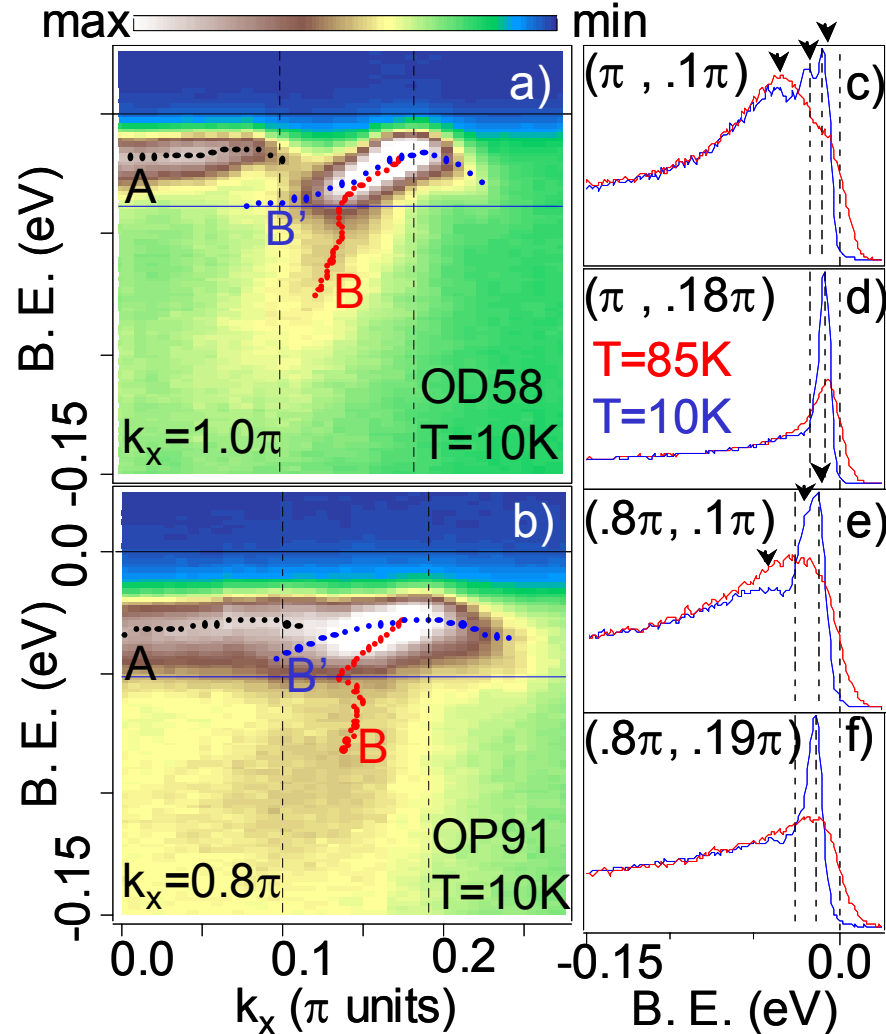
Normal and
superconducting state data
at different locations in the
Brillouin zone



Optimally doped sample, $T_C = 91$ K



Deconvolving peak dip hump structure due to the strong coupling and bi-layer splitting



Summary of the energy scales

